# POLITECNICO DI TORINO

Corso di Laurea Magistrale in
**Ingegneria Meccanica**

Tesi di Laurea Magistrale

# Experimental identification of the joints stiffness of the UR5 robot arm

**Relatore**
Prof. Stefano Pastorelli

*firma del relatore (dei relatori)*

……………………………

**Relatori UPC-Etseib**
Prof. J. Martínez
Prof. Mª A. de los Santos

**Candidato**
Giuseppe Testa

*firma del candidato*

.............................

A.A.2017/2018

# Abstract

This thesis work was born from the need to investigate the stiffness parameters of a robotic structure, which are not provided by the manufacturer.

The robot considered in this work is a light weight robot, the UR5 manipulator, whose characteristics are:

- Reduced weight (18.4 kg);
- High slenderness links, i.e. length ratio on high diameter;
- Notably flexible joints;

As a consequence of these characteristics, it is of fundamental importance to perform a modal analysis. In fact, vibrational phenomena can arise in robots with a low stiffness of both joints and links, and influence their performance, such as the precision of the movements. Therefore, as known, the stiffness analysis is preliminary to the modal analysis.

According to the hypothesis, the link stiffness has been considered infinite compared to the joint stiffness and therefore the aim of this thesis is to develop a simple experimental methodology for the identification of joint stiffness. Subsequently the results obtained by the developed method were compared with a method already adopted by the scientific community.

The structure of the thesis is divided into 6 chapters, as follows:

1. Introduction to the factors that influence stiffness in robotic structures;
2. Overview of physical and mathematical knowledge on which the study of stiffness is based;
3. State of the art in the methods of stiffness evaluation;
4. Overview of components used for the evaluation of joint stiffness in the laboratory;
5. Values of the stiffness in the UR5 joints obtained through the previously adopted methodology and the developed methodology;
6. Conclusions.

# Summary

# Introduction

The Stiffness can be defined as the capacity of a mechanical system to sustain loads without excessive changes of its geometry.

When a force is applied at the endpoint of a manipulator's arm, the endpoint will deflect by an amount which depends on the stiffness of the arm and the force applied. The stiffness of the arm's endpoint is determined by the stiffness of the manipulator's arm components and, more importantly, the positioning accuracy in the presence of disturbance forces and loads.

The stiffness analysis is of primary importance in order to guarantee the proper use of a robot and in order to design robotic systems, which must be suitable for a specific application.

In Robotics the principal works relating to stiffness may be classified according to four approach viewpoints:

1. The first approach deals with the determination of overall stiffness of the robotic system. Considering the stiffness of the robotic system such as motors, joints and link, the overall stiffness has to be determined. Consequently the stiffness evaluation, performance and stability considerations can be deduced;[1][2]

2. The second type studies the inverse decomposition of a stiffness matrix into constituent stiffness parameters that are often assumed to be simple linear springs or torsional springs; [3][4]

3. In the third approach, mathematical properties of the stiffness matrix are examined, with the main goal of finding intrinsic properties that are independent of the coordinate frame in which the stiffness matrix is expressed; [5][6]

4. The fourth type deals with the experimental evaluation of the stiffness performance of manipulator robotic systems. Different types of experimental tests have been proposed and, in some cases, they can be compared with theoretical results. [7][8]

There are still open problems related to stiffness. For example, the problem of improving the stiffness analysis in order to have a better match between theoretical and experimental results has not been completely solved.

This work was developed in the department of mechanical engineering. in UPC-ETSEIB of Barcelona during the Erasmus year (2016-2017), under the supervision of professors Prof. J. Martínez and Prof. Mª A. de los Santos. The project was designed during the first semester, after the student has acquired the main notions of robotics, and the project, it started in February 2017. A special word of thanks to Universitat politécnica de Catalunya and the supervisors that have made possible use of the laboratory and the necessary equipment in order to develop the project.

## Goal of the project

The main objective is to develop a simple experimental methodology for the joint stiffness identification and its application to a UR5 robot. This objective includes the validation of the methodology comparing redundant measurements obtained by using different sensors and measurement treatments. Such validation probably implies the use of a kinematic model of the robot described with the Jacobian matrix. The development of a dynamic model for the robot is out of the scope of this proposal.

# 1 Introduction to industrial manipulators.

Industrial manipulators are robot with a mechanical arm, wrist and gripper operating under computer control. The task of the robot manipulator is to place an object grasped by the gripper into an arbitrary pose .

The mechanical structure of a robot manipulator consists of a sequence of rigid bodies (links) interconnected by means of articulations (joints). A manipulator is characterized by an arm that ensures mobility, and a wrist that confers dexterity.

The task of the robot wrist is to enable the required orientation of the object grasped by the robot gripper, and an end-effector that performs the task required of the robot. The fundamental structure of a manipulator is the serial or open kinematic chain. From a topological viewpoint, a kinematic chain is termed open when there is only one sequence of links connecting the two ends of the chain. Alternatively, a manipulator contains a closed kinematic chain when a sequence of links forms a loop.

A manipulator's mobility is ensured by the presence of joints. The articulation between two consecutive links can be realized by means of either a prismatic or a revolute joint. The manipulator considered in this thesis has solely rotary, also called revolute, joints.

In an open kinematic chain, each prismatic or revolute joint provides the structure with a single degree of freedom(DOF). A prismatic joint creates a relative translational motion between the two links. Revolute joints are usually preferred to prismatic joints in view of their compactness and reliability. On the other hand, in a closed kinematic chain, the number of DOFs is less than the number of joints in view of the constraints imposed by the loop.

The degrees of freedom should be properly distributed along the mechanical structure in order to have a sufficient number to execute a given task. In the most general case of a task consisting of arbitrarily positioning and orienting an object in three-dimensional (3D) space, six DOFs are required, three for positioning a point on the object and three for orienting the object with the respect to a reference coordinate frame. If more DOFs than task variables are available, the manipulator is said to be redundant from a kinematic

viewpoint. The workspace represents portion of the environment where the manipulator's end-effector can access. Its shape and volume depend on the manipulator structure as well as on the presence of mechanical joint limits. The required task of the arm is to position the wrist which is then required to orient the end-effector. The type and sequence of the arm's DOFs, starting from the base joint, allows a classification of manipulators as Cartesian (figure 1), cylindrical (figure 2), spherical (figure 3), SCARA (figure 4) and anthropomorphic (figure 5).

According to the latest report by the International Federation of Robotics (IFR), up to 2005, 59% of installed robot manipulators worldwide has anthropomorphic geometry, 20% has Cartesian geometry, 12% has cylindrical geometry, and 8% SCARA geometry.
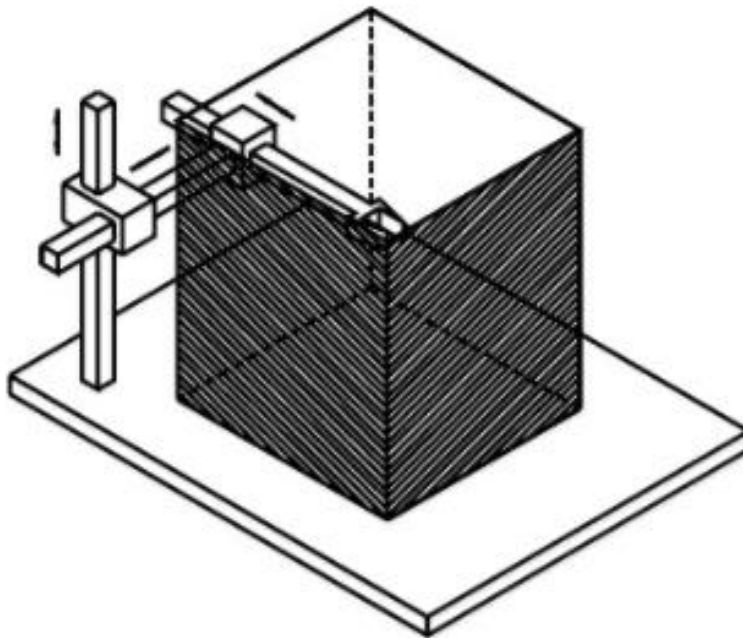


Figure 1 - Cartesian manipulator and its workspace [9].
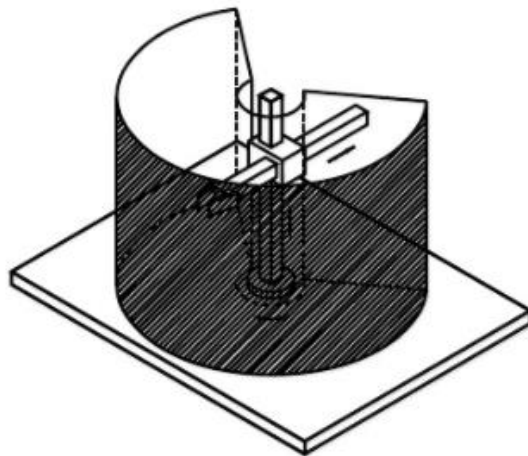
*Figure 2 - Cylindrical manipulator and its workspace [9]*
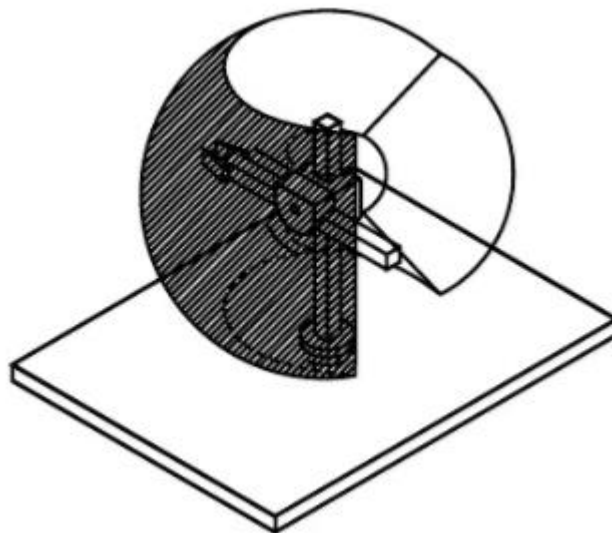


*Figure 3 - Spherical manipulator and its workspace [9].*

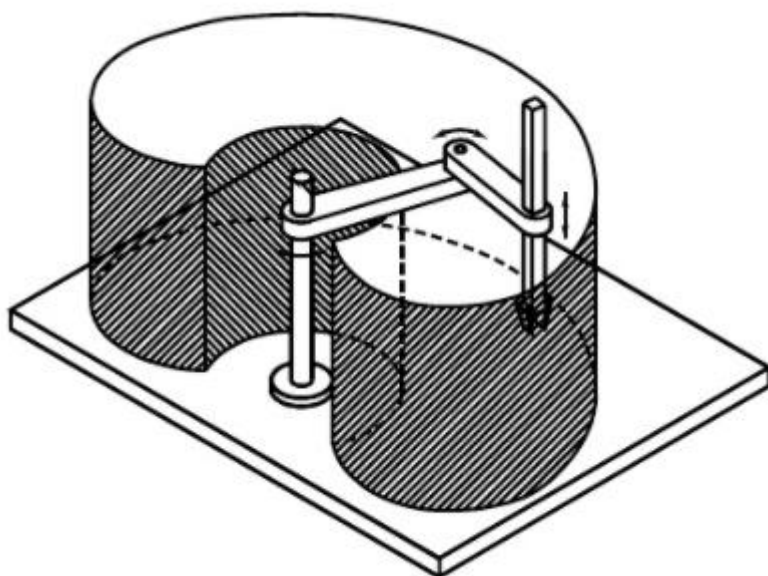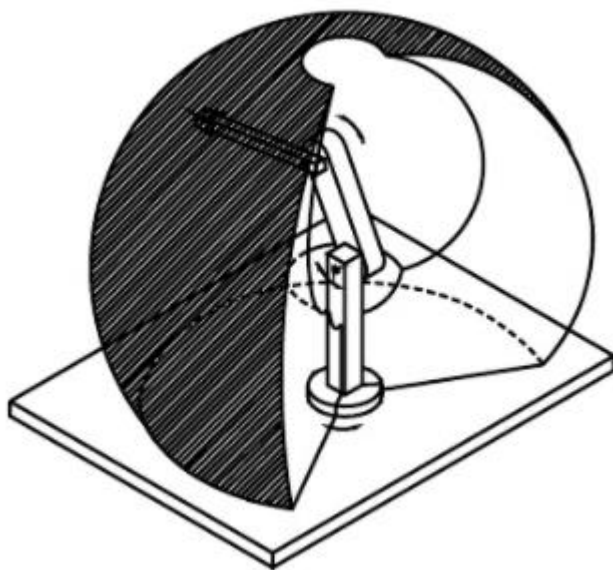*Figure 4 -  SCARA manipulator and its workspace [9].*



*Figure 5 - Anthropomorphic Manipulator and its workspace [9].*

All the previous manipulators have an open kinematic chain. Whenever larger payloads are required, the mechanical structure will have higher stiffness to guarantee comparable positioning accuracy. In such a case, resorting to a closed kinematic chain is advised.

An interesting closed-chain geometry is parallel geometry which has multiple kinematic chains connecting the base to the end-effector. The fundamental advantage is seen in the high structural stiffness, with respect to open-chain manipulators, and thus the possibility to achieve high operational speeds; the drawback is that of having a reduced workspace.

The manipulator structures presented above are required to position the wrist which is then required to orient the manipulator's end-effector. If arbitrary orientation in 3D space is desired, the wrist must possess at least three DOFs provided by revolute joints. Since the wrist constitutes the terminal part of the manipulator, it has to be compact; this often complicates its mechanical design. Without entering into construction details, the realization endowing the wrist with the highest dexterity is one where the three revolute axes intersect at a single point. In a case like that, the wrist is called a spherical wrist. The key feature of a spherical wrist is the decoupling between position and orientation of the end-effector; the arm is entrusted with the task of positioning the above point of intersection, whereas the wrist determines the end-effector orientation.

Realizations where the wrist is not spherical are simpler from a mechanical viewpoint, but position and orientation are coupled, and this complicates the coordination between the motion of the arm and that of the wrist to perform a given task. The end-effector is specified according to the task the robot should execute. For material handling tasks, the end-effector consists of a gripper of proper shape and dimensions determined by the object to be grasped. For machining and assembly tasks, the end-effector is a tool or a specialized device, a welding torch, a spray gun, or a screwdriver.

The versatility and flexibility of a robot manipulator should not induce the conviction that all mechanical structures are equivalent for the execution of a given task. The choice of a robot is conditioned by the application which sets constraints on the workspace dimensions and shape, the maximum payload, positioning accuracy, and dynamic performance of a manipulator.

## 1.1 The factors which influence the robot stiffness[10]

The overall stiffness of a robotic system is determined with the stiffness of all components od the system of the robot structures; such as joints and transmissions. In the following

sections a description of the main robotics components and their stiffness influence is reported:

### 1.1.1   Robot structures;

All robot structures are flexible to a degree, some are substantially more flexible than others. Only two structural types, flexible and rigid, are considered here. Rigid structures are defined as those for which both the kinematic solution and the control algorithms assume all links to be rigid. Most commercially available robot arms are of this type. Control of these rigid manipulators assumes that there is no structural deflection, whereas in fact, for certain loading conditions, system deflections can be significant and will result in decreased accuracy.

The most important performance characteristics for robot structures are stiffness in bending and in torsion. Inadequate structural stiffness can also adversely affect overall manipulator precision. The two most common types of structures for robot manipulator's arms are monocoque or shell structures and beam structures. Although the monocoque structures have lower weight or higher strength-to-weight ratios, they are more expensive and generally more difficult to manufacture. The structure stiffness is affected also by the choice of method of manufacturing and the material, typical designs include bolted, welded assemblies, and epoxied assembling ies of cast elements.

Instead the most common materials for robot structures used are aluminum and steel, although thermoplastics and glass or carbon-fiber reinforced plastics are beginning to be used.

### 1.1.2   Robot joints;

Robotic joints can be categorized generally as either prismatic or revolute joints. Other types, such as spherical or universal joints, the latter are generally implemented as combinations of the two primary classes.
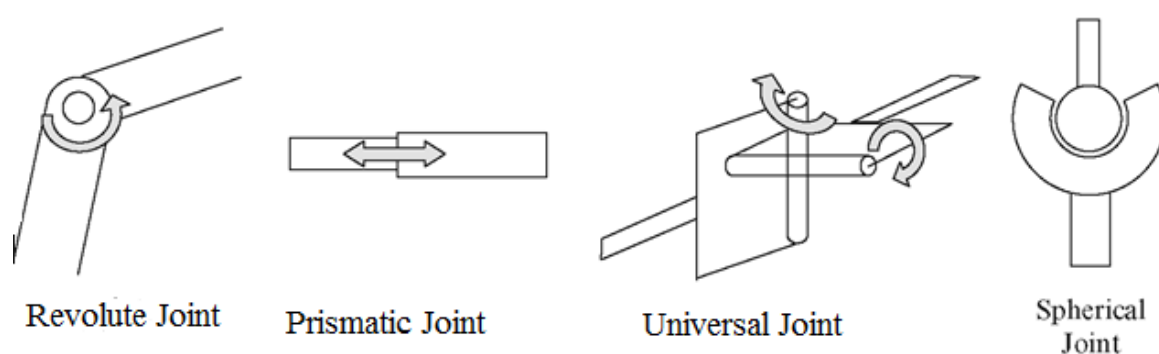
*Figure 6- Symbolic representation of joints*

There are two basic types of prismatic or linear motion joints: single-stage and multiple-stage or telescoping joints. Single-stage joints are made up of a moving surface that slides linearly along a fixed a surface. Multiple-stage joints are actually sets of nested or stacked single-stage joints (Multiple-stage joints di single stage joints). Single-stage joints feature simplicity and high stiffness, whereas the primary advantage of telescoping joints is their retracted-state compactness and large extension ratio. Telescoping joints have a lower joint inertia for some motions because part of the joint may remain stationary. In prismatic joints are employed the bearings with the primary function to facilitate motion in a single direction and to prevent motion in all other directions, both linear and rotational. Preventing these unwanted motions poses the more challenging design problem. Deformations in the structure can significantly affect bearing surface configuration, which affects performance. In severe cases, roller deflection under load may cause binding, which precludes motion. For high-precision prismatic joints, ways must be made straight over long distances. The required precision grinding on multiple surfaces can be expensive.

The primary criterion for evaluating prismatic joints is the stiffness-to-weight ratio. Achieving a good stiffness-to-weight ratio requires the use of hollow structure for the moving elements rather than solid rods. Bearing spacing is extremely important in design for stiffness. If spacing is too short, system stiffness will be inadequate to matter how great the bearing stiffness. Major causes for failure in prismatic joints are foreign particle contamination and Brinelling of the ways caused by excessive ball loading and by shock loads.

Revolute ( rotary motion) joints are designed to allow pure rotation while minimizing radial and axial motions. There are many design issues to be considered when designing a revolute joint. The most important measure of the quality of a revolute joint is its stiffness or resistance to all undesired motion. Key factors to be considered in design for stiffness are bearing shaft, housing and diameters, clearances and tolerances, mounting configuration of the bearings, and implementation of proper bearing preloading. Bearing size is not always based on load-carrying capacity; rather, the bearing chosen often will be smallest one that is stiff enough in both bending and torsion to give desired system stiffness that will fit on the shaft. Because joint shafts will frequently be torque-transmitting members, they must be designed both for bending and torsional stiffness.

An important factor in maintaining stiffness in a revolute joint is choice of bearing-mount(support) configuration. The interface between the mount and the structure is as important as the interface between the mount and the bearing. The mount and mounting arrangement must also be designed to accommodate preloading of the bearings. Axial preloading of ball or tapered roller bearings improves system accuracy and stiffness by minimizing bearing radial and axial play. Preloads can be achieved through the use of selective assembly or spring elements, shim spacers, or threaded collars.

### 1.1.3   Transmissions;

Many types of transmission elements are in use in robot design. The purpose of the transmission is to transmit mechanical power from a source to a load. Choice of transmission elements depends on power requirements, the nature of the desired motion, and the placement of the power source with respect to the joint. The primary considerations in transmission design are stiffness, efficiency and cost.

Today the most common transmission elements in robots are gears, helical gears are also used in robot transmissions. They have several specific advantages. Because gear reductions are often quite large in robot transmissions, lack of adequate gear tooth contact ratio can be a problem. For given gear ratios and gear sizes, helical gears have higher contact ratios and as a result produce smoother output. They also tend to be quieter. The primary disadvantage to helical gears is that they produce axial gear loads that must be constrained to maintain drive stiffness. The limiting factor in gear transmission stiffness is

the stiffness of the gear teeth; each tooth acts as an elastic cantilever during the time that it is loaded. To maximize stiffness, the largest possible gear diameters should be chosen.

Another common linear motion transmission element in robot design is the ball screw. Ball screws feature high efficiency, moderate stiffness, and short leads which offer large mechanical advantages. Screws can be purchased both in precision (ground) and commercial (rolled) grades. Precision ball screws are purchased with ball nuts as matching pairs.

Normally the most common transmission element in revolution joints is the Harmonic Drive, a patented unit (USM Corp.). These drives feature in-line parallel shafts and very high transmission ratios in compact packages. Static friction in these drives is high, and manufacturing tolerances often result in cyclic friction torque variation called cogging. Power is often transmitted in robots through torsion shafts or weight-saving torque tubes. Transmitting power at high angular velocities also minimizes required shaft diameter, wall thickness, and weight.

Several robot manufacturers use timing belts as transmission elements. They are used primarily when low-cost power transmission is required over large distances, or as a simple interface between the motor and the first stage of gear reduction. Transmission ratios are limited because there is generally a minimum pulley size based on the belt fatigue life. Drive stiffness in a belt transmission is a function of the belt material and belt tensioning system. Belts containing fine fibers of materials such as Kevlar, which have high stiffness modulus to weight ratios, can be driven around smaller pulleys because the Kevlar reinforcing bands themselves consist of flexible microscopic fibers.

A common transmission element in low-cost robots is the stranded cable or flat alloy steel band. These elements are easy to configure and repair and relatively efficient. Stiffness in cables and bands, as with stiffness in belts, is primarily a function of the choice of material.

# 2   Modeling of industrial Manipulators.

To address the problem of stiffness, with all the necessary means, in this section gives an introduction to the modeling of industrial manipulators, by setting the notations and the parameters that are used.

The axis of rotation of a revolute joint, denoted by $z_i$, is the interconnection of links $l_i$ and $l_{i+1}$. The joint variables, denoted by $q_i$, represent the relative displacement between adjacent links. As the joints in this study are revolute, it holds in this special case that $q_i = \vartheta_i, \forall\, i \in \{1, \dots, n\}$, where $\vartheta_i$ denotes a relative rotation. Both notations are used throughout the thesis.
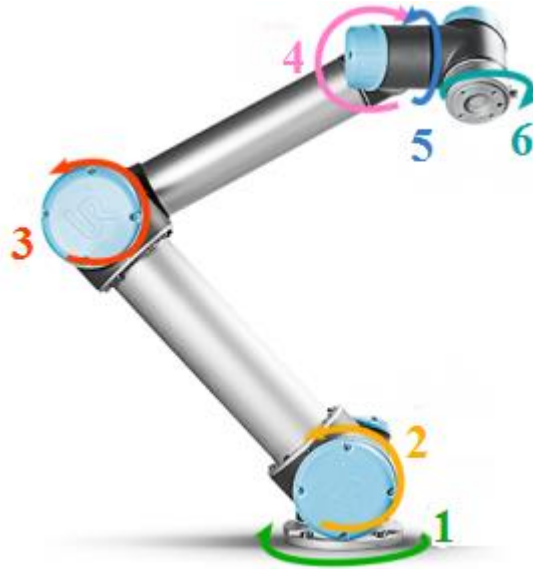


*Figure 7- UR5 Joints[11]*

The specification of the location of every point on the manipulator is called the configuration of the robot. The set of all configurations is called the configuration space. As the base of manipulators is commonly fixed and the links are assumed to be rigid, the configuration is defined by knowing the values of the joint variables. These are often gathered into a vector $q = [q_1, \dots, q_n]^T$. The joint velocities are then $\dot{q} = [\dot{q}_1, \dots, \dot{q}_n]^T$. The following section gives an introduction to the modeling of industrial manipulators.

The modeling of manipulators is often simplified to step-by-step procedures. Rigid motions and homogeneous transformation are defined to represent the positions and orientations of objects and the rotation and translation between assigned coordinate frames.

A method called the Denavit-Hartenberg (DH) convention was developed to standardize the assignment of coordinate frames to joints and links of manipulators and to create homogeneous transformation matrices. By using those matrices it is easy to derive the forward kinematics. In order to derive the velocity kinematics a Jacobian is defined specifically for robotic manipulators, also called the manipulator Jacobian and either the Euler-Lagrange equations or the Newton-Euler formulation it is possible to derive the dynamic equations for the manipulators.

## 2.1 Rigid motions and homogeneous transformations

Rigid motions and homogeneous transformations are used to describe the relative positions and orientations between the coordinate systems that are assigned to each joint and its respective link. Homogeneous transformations combine the operations of rotation and translation into a single matrix multiplication which is commonly used to derive the forward kinematic equations of rigid manipulators and to perform coordinate transformations. Rigid motions are defined to be an ordered pair $(t, R)$ where $t \in \mathbb{R}^3$ is a translation vector and $R \in SO(3)$ is a rotation matrix of the Special Orthogonal group of order three, where $SO(m)$ is the special orthonormal group of the real matrices with orthonormal columns and determinant equal to 1, in the case of spatial rotations it is m=3. Rotation matrices can be used to represent the orientation of one coordinate frame with respect to another as well as to transform the coordinates of a point from one frame to another. Successive rotations such as a rotational transformation of a frame $o_i x_i y_i z_i$ to a frame $o_j x_j y_j z_j$ and further to frame $o_k x_k y_k z_k$ can be obtained by

$$R_k^i = R_j^i R_k^j \qquad (1)$$

where the subscripts indicate from which system of reference the rotation matrix is referred and the apexes indicate to which system of reference the rotation matrix is referred.

Homogeneous transformations simplify the handling of long sequences of rigid motions, as it reduces the composition of rigid motions to matrix multiplication. A homogeneous transformation matrix $A \in \mathbb{R}^{4x4}$ has the form of

$$A = \begin{bmatrix} R & t \\ 0 & 1 \end{bmatrix}, R \in SO(3), d \in \mathbb{R}^3 \qquad (2)$$

Using the fact that **R** is orthogonal the inverse of the homogeneous transformation matrix is simply

$$A^{-1} = \begin{bmatrix} R^T & -R^T t \\ 0 & 1 \end{bmatrix} \qquad (3)$$

To calculate subsequent transformations, the homogeneous transformation matrices must be multiplied, according to

$$T_j^i = A_{i+1}^i \dots A_j^{j-1} \qquad (4)$$

The rotational parts are then given by

$$R_j^i = R_{i+1}^i \dots R_j^{j-1} \qquad (5)$$

and the translation vectors are given by

$$d_j^i = d_{i-1}^i + R_{j-1}^i d_j^{j-1} \qquad (6)$$

Building upon the definitions of rigid motions and homogeneous transformation, the forward kinematics can be calculated, as shown in the next section.

## 2.2 Kinematic

Kinematics is the science of motion that treats the subject without regard to the forces that cause it. Within the science of kinematics, one studies the position, the velocity, the acceleration, and all higher order derivatives of the position variables. Hence, the study of the kinematics of manipulators refers to all the geometrical and time-based properties of the motion. In order to deal with the complex geometry of a manipulator, we affix frames to the various parts of the mechanism and then describe the relationships between these frames. The study of manipulator kinematics involves among other things, how the locations of these frames change as the mechanism articulates. The central topic of this chapter is a method to compute the position and orientation of the manipulator's end-effector relative to the base of the manipulator as a function of the joint variables. The DH convention and a few other definitions help to assign the coordinate systems in a standardized way and are presented in the following section.

### 2.2.1 Introduction

Consider an open-chain manipulator constituted by $n+1$ links connected by $n$ joints, where Link 0 is conventionally fixed to the ground. It is assumed that each joint provides the mechanical structure with a single DOF, corresponding to the joint variable. The construction of an operating procedure for the computation of direct kinematics is naturally derived from the typical open kinematic chain of the manipulator structure. In fact, since

each joint connects two consecutive links, it is reasonable to consider first the description of kinematic relationship between consecutive links and then to obtain the overall description of manipulator kinematics in a recursive fashion.
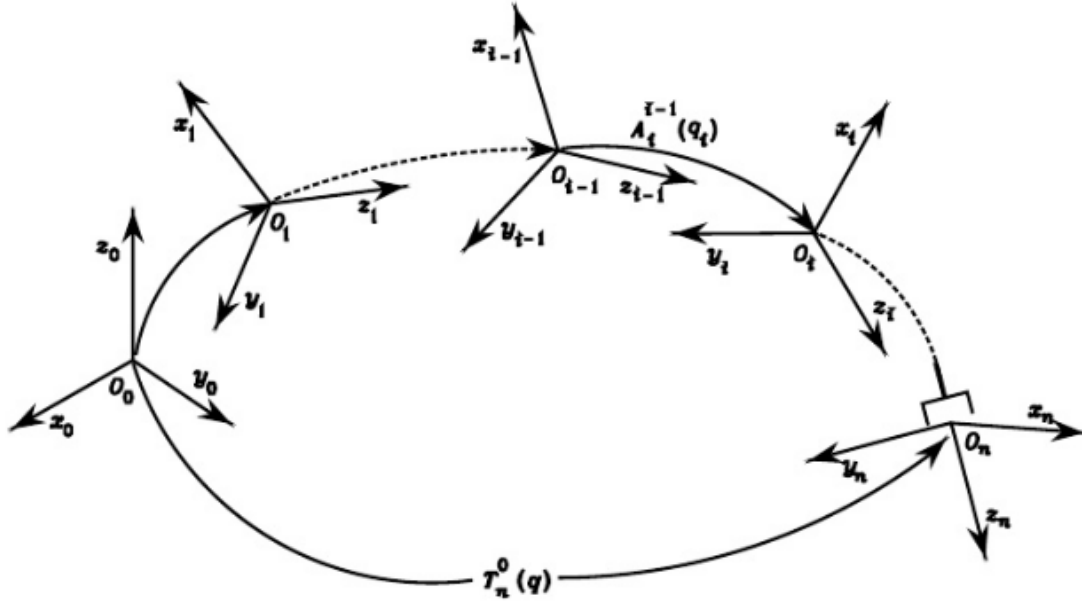


*Figure 8-Coordinate transformations in an open kinematic chain [9]*

To this purpose, it is worth defining a coordinate frame attached to each link, from Link 0 to Link *n*. Then, the coordinate transformation describing the position and orientation of Frame *n* with respect to Frame 0 (Figure 8) is given by

$$T_n^0(q) = A_1^0(q_1)A_2^1(q_2) \dots A_n^{n-1}(q_n) \tag{7}$$

As requested, the computation of direct kinematics function is recursive and is obtained in a systematic manner by simple products of the homogeneous transformation matrices $A_i^{i-1}(q_i)(for\ i = 1, \dots, n)$, each of which is a function of a single joint variable.

## 2.2.2   Denavit-Hartenberg Convention

In order to compute the direct kinematics equation for an open-chain manipulator according to the recursive expression in, a systematic, general method is to be derived to define the relative position and orientation of two consecutive links; the problem is that to

determine two frames attached to the two links and compute the coordinate transformations between them. In general, the frames can be arbitrarily chosen as long as they are attached to the link they are referred to. Nevertheless, it is convenient to set some rules also for the definition of the link frames.
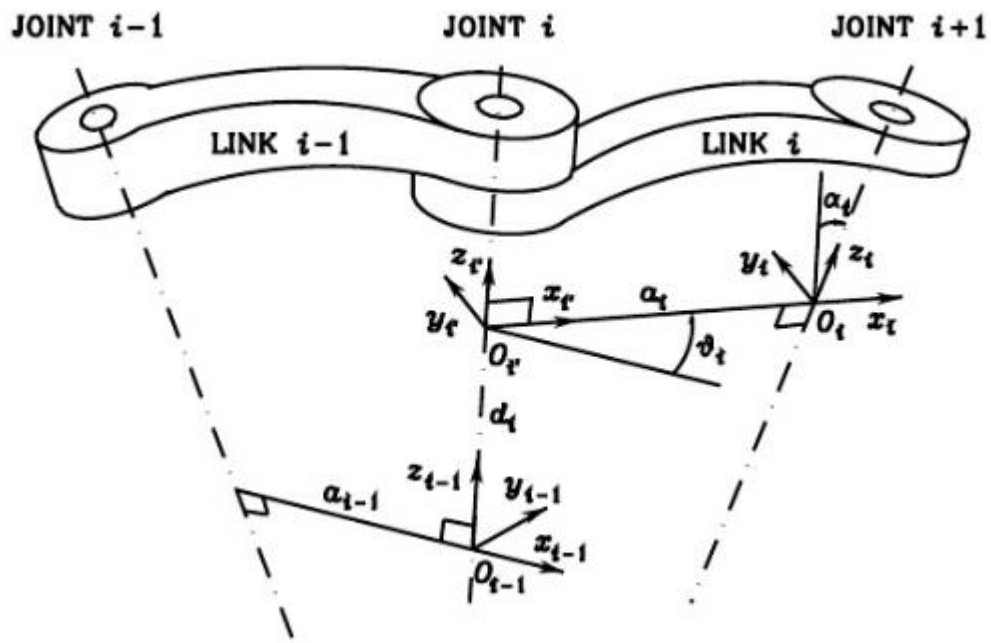


*Figure 9- Denavit-Hartenberg kinematic parameters [9]*

With reference to (Figure 9), let Axis $i$ denote the axis of the joint connecting Link $i$-1 to Link $i$; the so-called *Denavit-Hartenberg convention* (DH) is adopted to define link Frame $i$:

- Choose axis $z_i$ along the axis of Joint $i$+1;
- Locate the origin $O_i$ at the intersection of axis $z_i$ with the common normal ( the common normal between two lines is the line containing the minimum distance segment between the two lines) to axes $z_{i-1}$ and $z_i$. Also, locate $O_{i'}$ at the intersection of the common normal with axis $z_{i-1}$;
- Choose axis $x_i$ along the common normal to axes $z_{i-1}$ and $z_i$ with direction from joint $I$ to joint $i$+1;
- Choose axis $y_i$ so as to complete a right-handed frame.

The Denavit-Hartenberg convention gives a no-unique definition of the link frame in the following cases:

- For frame 0, only the direction of axis $z_0$ is specified; then $O_0$ and $x_0$ can be arbitrarily chosen;
- For frame $n$, since there is no Joint n+1, $z_n$ is not uniquely defined while $x_n$ has to be normal to axis $z_{n-1}$. Typically, Joint $n$ is revolute, and thus $z_n$ is to be aligned with the direction of $z_{n-1}$.
- When two consecutive axes are parallel, the common normal between then is not uniquely defined;
- When two consecutive axes intersect, the direction of $x_i$ is arbitrary;
- When Joint $I$ is prismatic, the direction of $z_{i-1}$ is arbitrary.

In all such cases, the indeterminacy can be exploited to simplify the procedure; for instance, the axes of consecutive frames can be made parallel. Once the link frames have been established, the position and orientation of Frame $i$ with respect to Frame $i$-1 are completely specified by the following parameters:

- $a_i$ distance between $O_{i'}$;
- $d_i$ coordinate of $O_{i'}$ along $z_{i-1}$;
- $\alpha_i$ angle between axes $z_{i-1}$ and $z_i$ about axis $x_i$ to be taken positive when rotation is made counter-clockwise;
- $\theta_i$ angle between axes $x_{i-1}$ and $x_i$ about axis $z_{i-1}$ to be taken positive when rotation is made counter-clockwise. As all the joints in the UR5 are revolute, $\theta_i$ is a variable.

Two of four parameters ($a_i$ and $\alpha_i$) are always constant and depend only on the geometry of connection between consecutive joints established by Link $i$. Of remaining two parameters, only one is variable depending on the type of that joint that connects Link $i$-1. In particular:

- If joint $i$ is revolute the variable is $\theta_i$;
- If joint $i$ is prismatic the variable is $d_i$;

At this point, it is possible to express the coordinate transformation between Frame $i$ and Frame $i$-1 according to following steps:

- Choose a frame aligned with Frame *i-1*;

- Translate the chosen frame by $d_i$ along axis $z_{i-1}$ and rotate it by $\theta_i$ about axis $z_{i-1}$; this sequence aligns the current frame with Frame $i'$ and is described by the homogeneous transformation matrix:

$$A_{i'}^{i-1} = \begin{bmatrix} \cos\theta_i & -\sin\theta_i & 0 & 0 \\ \sin\theta_i & \cos\theta_i & 0 & 0 \\ 0 & 0 & 1 & d_i \\ 0 & 0 & 0 & 1 \end{bmatrix} \qquad (8)$$

- Translate the frame aligned with Frame *i'* by $a_i$ along axis $x_{i'}$ and rotate it by $\alpha_i$ about axis $x_{i'}$; this sequence aligns the current frame with Frame *i* and is described by the homogeneous transformation matrix

$$A_i^{i'} = \begin{bmatrix} 1 & 0 & 0 & a_i \\ 0 & \cos\alpha_i & -\sin\alpha_i & 0 \\ 0 & \sin\alpha_i & \cos\alpha_i & 0 \\ 0 & 0 & 0 & 1 \end{bmatrix} \qquad (9)$$

- The resulting coordinate transformation is obtained by post multiplication of the single transformations as

$$A_i^{i-1} = A_{i'}^{i-1} A_i^{i'} = \begin{bmatrix} \cos\theta_i & -\sin\theta_i\cos\alpha_i & \sin\theta_i\sin\alpha_i & a_i\cos\theta_i \\ \sin\theta_i & \cos\theta_i\cos\alpha_i & -\cos\theta_i\sin\alpha_i & a_i\sin\theta_i \\ 0 & \sin\alpha_i & \cos\alpha_i & d_i \\ 0 & 0 & 0 & 1 \end{bmatrix} \qquad (10)$$

Notice that the transformation matrix from Frame *i* to Frame *i-1* is a function only of the joint variable $q_i$, that is, $\theta_i$ for a revolute joint or $d_i$ for a prismatic joint.

### 2.2.3   Differential Kinematics and Statics

The differential kinematics is gives the relationship between the joint velocities and the corresponding end-effector linear and angular velocity. This mapping is described by a matrix, termed *geometric Jacobian,* which depends on the manipulator configuration. Alternatively, if the end-effector pose is expressed with reference to a minimal representation in the operational space, it is possible to compute the Jacobian matrix via

differentiation of the direct kinematics function with respect to the joint variables. The resulting Jacobian, termed *analytical Jacobian,* in general differs from the geometric one. The Jacobian constitutes one of the most important tools for manipulator characterization; in fact, it is useful for finding singularities, analyzing redundancy, determining inverse kinematics algorithms, describing the mapping between forces applied to the end-effector and resulting torques at the joints (statics) and, as will be seen in the following section.

### 2.2.3.1 Geometric Jacobian

Consider an *n*-DOF manipulator. The direct kinematics equation can be written in the form, as seen above:

$$T_e(q) = \begin{bmatrix} R(q) & p(q) \\ 0 & 1 \end{bmatrix} \qquad (11)$$

the subscript indicate that the matrix is referred to end effector:



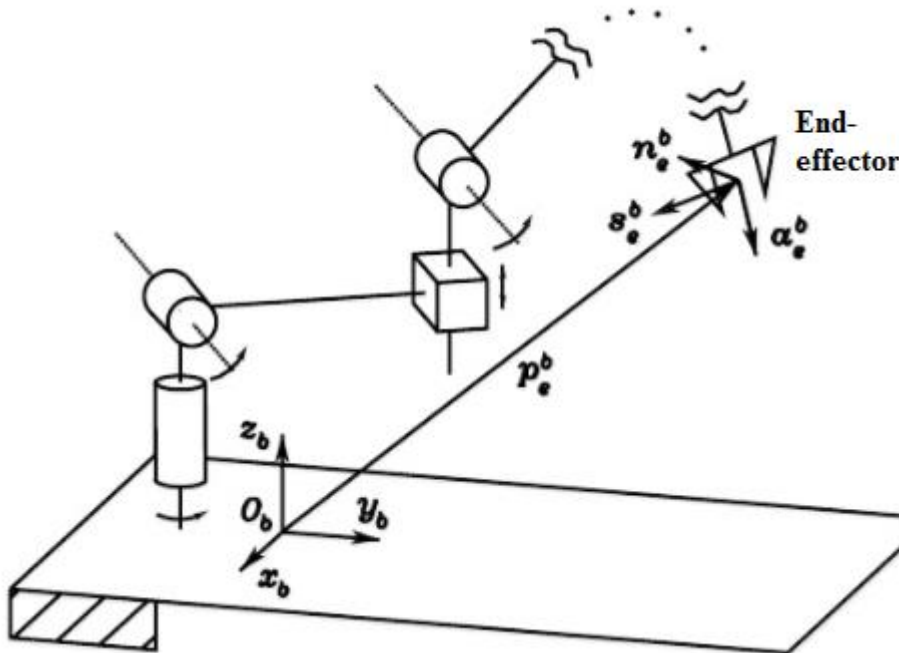*Figure 10- End effector reference[9]*

Where $q = [q_1 \dots q_n]^T$ is the vector of joint variables. Both end-effector position and orientation vary as $q$ varies. The goal of the differential kinematics is to find the

relationship between the joint velocities and the end-effector linear and angular velocities. In other words, it is desired to express the end-effector linear velocity $\dot{p}$ and angular velocity $\omega$ as a function of the joint velocities $\dot{q}$. As will be seen afterwards, the sought relations are both linear in the joint velocities,

$$\dot{p} = J_P(q)\dot{q} \tag{12}$$

$$\omega = J_O(q)\dot{q} \tag{13}$$

In the Equation (12) $J_P$ is the ($3 \times n$) matrix relating the contribution of the joint velocities $\dot{q}$ to the end-effector *linear* velocity $\dot{p}$, while in the Equation (13) $J_O$ is the ($3 \times n$) matrix relating the contribution of the joint velocities $\dot{q}$ to the end-effector *angular* velocity $\omega$. In compact form, the equation (12) and (13) can be written as

$$v = \begin{bmatrix} \dot{p} \\ \omega \end{bmatrix} = J(q)\,\dot{q} \tag{14}$$

Which represent the manipulator *differential kinematics equation.* The ($6 \times n$) matrix **J** is the manipulator *geometric Jacobian*

$$J = \begin{bmatrix} J_P \\ J_O \end{bmatrix} \tag{15}$$

which in general is a function of the joint variables.

In order to compute the geometric Jacobian, it is worth recalling a number of properties of rotation matrices and some important results of rigid body kinematics.

### 2.2.3.1.1  Derivate of a Rotation Matrix

The manipulator direct kinematics equation in (11) describes the end-effector pose, as a function of the joint variables, in terms of a position vector and a rotation matrix. Since the aim is to characterize the end-effector linear and angular velocities, it is worth considering first the *derivative of a rotation matrix* with respect to time.

Consider a time-varying rotation matrix $R=R(t)$. In view of the orthogonality of $R$, one has the relation

$$R(t)R^T(t) = I \qquad (16)$$

which, differentiated with respect to time, gives the identity

$$\dot{R}(t)R^T(t) + R(t)\dot{R}^T(t) = O \qquad (17)$$

Set

$$S(t) = \dot{R}(t)R^T(t) \qquad (18)$$

the (3×3) matrix $S$ is *skew-symmetric* since

$$S(t) + S^T(t) = O \qquad (19)$$

Postmultiplying both sides of (18) by $R(t)$ gives

$$\dot{R}(t) = S(t)R(t) \qquad (20)$$

that allows the time derivative of $R(t)$ to be expressed as a function of $R(t)$ itself. Equation (20) relates the rotation matrix $R$ to its derivative by means of the skew-symmetric operator $S$ and has a meaningful physical interpretation. Consider a constant vector $p'$ and the vector $p(t)= R(t)\ p'$. The time derivative of $p(t)$ is

$$\dot{p}(t) = \dot{R}(t)p' \qquad (21)$$

which, in view of (20), can be written as

$$\dot{p}(t) = S(t)R(t)\ p' \qquad (22)$$

If the vector $\omega(t)$ denotes the *angular velocity* of frame $R(t)$ with respect to the reference frame at time $t$, it is known from mechanics that

$$\dot{p}(t) = \omega(t) \times R(t)\ p' \qquad (23)$$

Therefore, the matrix operator $S(t)$ describes the vector product between the vector $\boldsymbol{\omega}$ and the vector $\boldsymbol{R}(t)\,\mathbf{p'}$. The matrix $S(t)$ is so that its symmetric elements with respect to the main diagonal represent the components of the vector $\boldsymbol{\omega}(t) = [\omega_x \quad \omega_y \quad \omega_z]^T$ in the form

$$S = \begin{bmatrix} 0 & -\omega_z & \omega_y \\ \omega_z & 0 & -\omega_x \\ -\omega_y & \omega_x & 0 \end{bmatrix} \qquad (24)$$

Which justifies the expression $S(t) = S(\boldsymbol{\omega}(t))$. Hence,(20) can be rewritten as

$$\dot{R}(t) = S(\omega)R \qquad (25)$$

Furthermore, if $\mathbf{R}$ denotes a rotation matrix, it can be shown that the following relation holds:

$$RS(\omega)R^T = S(R\omega) \qquad (26)$$

Which will be useful later
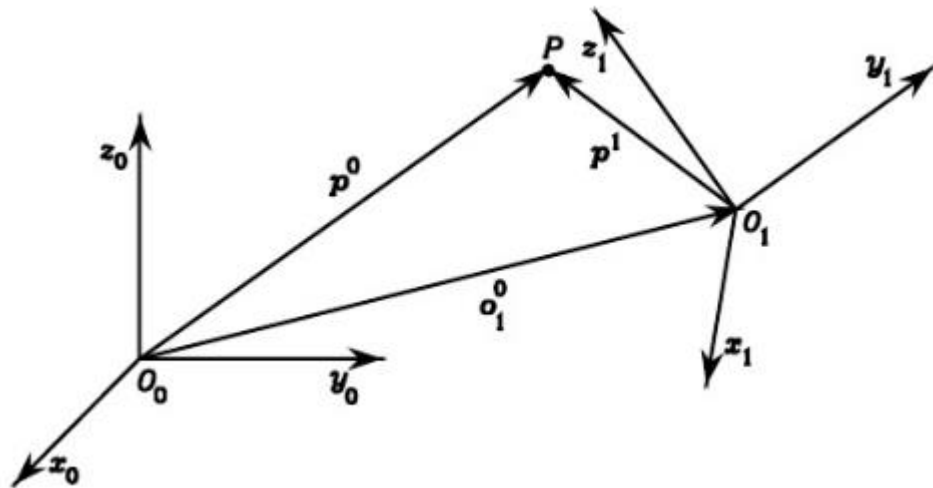


*Figure 11- Representation of a point P in different coordinate frames [9]*

With reference to (Figure 11), consider the coordinate transformation of a point P from Frame 1 to Frame 0;

$$\boldsymbol{p}^0 = \boldsymbol{o}_1^0 + \boldsymbol{R}_1^0 \boldsymbol{p}^1 \tag{27}$$

Differentiating (27) with respect to time gives

$$\dot{\boldsymbol{p}}^0 = \dot{\boldsymbol{o}}_1^0 + \boldsymbol{R}_1^0 \dot{\boldsymbol{p}}^1 + \dot{\boldsymbol{R}}_1^0 \boldsymbol{p}^1 \tag{28}$$

utilizing the expression of the derivative of a rotation matrix (20) and specifying the dependence on the angular velocity gives

$$\dot{\boldsymbol{p}}^0 = \dot{\boldsymbol{o}}_1^0 + \boldsymbol{R}_1^0 \dot{\boldsymbol{p}}^1 + \boldsymbol{S}(\boldsymbol{\omega}_1^0) \boldsymbol{R}_1^0 \boldsymbol{p}^1 \tag{29}$$

Further, denoting the vector $\boldsymbol{R}_1^0 \boldsymbol{p}^1$ by $\boldsymbol{r}_1^0$, it is

$$\dot{\boldsymbol{p}}^0 = \dot{\boldsymbol{o}}_1^0 + \boldsymbol{R}_1^0 \dot{\boldsymbol{p}}^1 + \boldsymbol{\omega}_1^0 \times \boldsymbol{r}_1^0 \tag{30}$$

which is the known form of the velocity composition rule.

Notice that, if $\boldsymbol{p}^1$ is *fixed* in Frame 1, then it is

$$\dot{\boldsymbol{p}}^0 = \dot{\boldsymbol{o}}_1^0 + \boldsymbol{\omega}_1^0 \times \boldsymbol{r}_1^0 \tag{31}$$

Since $\dot{\boldsymbol{p}}^1 = 0$.

### 2.2.3.1.2 Link Velocities

Consider the generic Link *I* of a manipulator with an open kinematic chain. According to the Denavit-Hartenberg convention adopted in the previous chapter, Link *I* connects Joints *i* and *i+1*; Frame *I* is attached to Link *I* and has origin along Joint *i+1* axis, while Frame *i-1* has origin along Joint *i* axis (Figure 10).
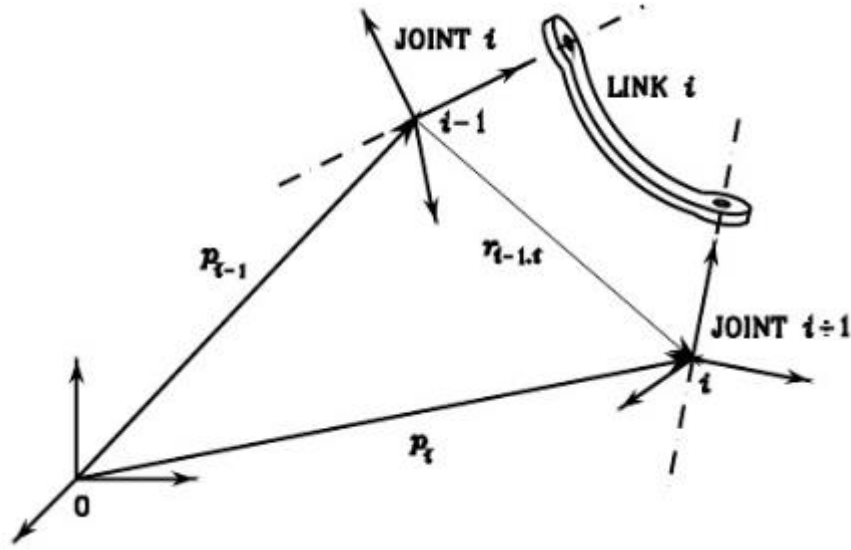
*Figure. 7-Characterization of generic Link i of a manipulator [9].*

Let $\boldsymbol{p}_{i-1}$ and $\boldsymbol{p}_i$ be the position vectors of the origins of Frames $i$-1 and $i$, respectively. Also, let $\boldsymbol{r}_{i-1,i}^{i-1}$ denote the position of the origin of Frame $i$ and with respect to Frame $i$-1. According to the coordinate transformation(25), one can write

$$\boldsymbol{p}_i = \boldsymbol{p}_{i-1} + \boldsymbol{R}_{i-1}\boldsymbol{r}_{i-1,i}^{i-1} \qquad (31)$$

Then, by virtue of (30), it is

$$\dot{\boldsymbol{p}}_i = \dot{\boldsymbol{p}}_{i-1} + \boldsymbol{R}_{i-1}\dot{\boldsymbol{r}}_{i-1,i}^{i-1} + \boldsymbol{\omega}_{i-1} \times \boldsymbol{R}_{i-1}\boldsymbol{r}_{i-1,i}^{i-1} = \dot{\boldsymbol{p}}_{i-1} + \boldsymbol{v}_{i-1,i} + \boldsymbol{\omega}_{i-1} \times \boldsymbol{r}_{i-1,i} \qquad (32)$$

Which gives the expression of the linear velocity of Link $i$ as a function of the translational and rotational velocities of Link $i$-1. Note that $\boldsymbol{v}_{i-1,i}$ denotes the velocity of the origin of Frame $i$ with respect to the origin of Frame $i$-1. Concerning link angular velocity, it is worth starting from the rotation composition

$$\boldsymbol{R}_i = \boldsymbol{R}_{i-1}\boldsymbol{R}_i^{i-1} \qquad (33)$$

from (20), its time derivative can be written as

$$\boldsymbol{S}(\boldsymbol{\omega}_i)\boldsymbol{R}_i = \boldsymbol{S}(\boldsymbol{\omega}_i)\boldsymbol{R}_{i-1} + \boldsymbol{R}_{i-1}\boldsymbol{S}(\boldsymbol{\omega}_{i-1,i}^{i-1})\boldsymbol{R}_i^{i-1} \qquad (34)$$

where $\boldsymbol{\omega}_{i-1,i}^{i-1}$, denotes the angular velocity of Frame $i$ with respect to Frame $i$-1 expressed in Frame $i$-1. Considering that $\mathbf{R}$ is an *orthogonal* matrix meaning that

$$R^T R = I_3 \tag{35}$$

where $I_3$ denotes the (3×3) identity matrix, then the second term on the right-hand side of (34) can be rewritten as

$$R_{i-1} S\big(\omega_{i-1,i}^{i-1}\big) R_i^{i-1} = R_{i-1} S\big(\omega_{i-1,i}^{i-1}\big) R_{i-1}^T R_{i-1} R_i^{i-1} \tag{36}$$

in view of property (26), it is

$$R_{i-1} S\big(\omega_{i-1,i}^{i-1}\big) R_i^{i-1} = S\big(R_{i-1} \omega_{i-1,i}^{i-1}\big) R_i \tag{37}$$

Then, (34) becomes

$$S(\omega_i) R_i = S(\omega_{i-1}) R_i + S\big(R_{i-1} \omega_{i-1,i}^{i-1}\big) R_i \tag{38}$$

leading to the result

$$\omega_i = \omega_{i-1} + R_{i-1} \omega_{i-1,i}^{i-1} = \omega_{i-1} + \omega_{i-1,i} \tag{39}$$

Which gives the expression of the angular velocity of Link *I* as a function of the angular velocities of Link *i*-1 and of Link *I* with respect to Link *i*-1. The relations (32),(39) attain different expressions depending on the type of Joint *i* (*prismatic* or *revolute*), in the case study of this work will be treated only Revolute Joint, given that the UR5 manipulator is composed of revolute Joint.

**Revolute joint**

For the angular velocity it is obviously

$$\omega_{i-1,i} = \dot{\vartheta}_i z_{i-1} \tag{40}$$

While for the linear velocity it is

$$v_{i-1,i} = \omega_{i-1,i} \times r_{i-1,i} \tag{41}$$

due to the rotation of Frame *i* with respect to Frame *i*-1 induced by the motion of Joint *i*. Hence, the expressions of angular velocity (39) and linear velocity (32) respectively become

$$\boldsymbol{\omega}_i = \boldsymbol{\omega}_{i-1} + \dot{\vartheta}_i \boldsymbol{z}_{i-1} \qquad (42)$$

$$\dot{\boldsymbol{p}}_i = \dot{\boldsymbol{p}}_{i-1} + \boldsymbol{\omega}_i \times \boldsymbol{r}_{i-1,i} \qquad (43)$$

where (39) has been exploited to derive (43).

### 2.2.3.1.3   Jacobian computation

In order to compute the Jacobian, it is convenient to proceed separately for the linear velocity and the angular velocity.

For the contribution to the linear velocity, the time derivative of $\boldsymbol{p}_e(\boldsymbol{q})$ can be written as

$$\dot{\boldsymbol{p}}_e = \sum_{i=1}^{n} \frac{\partial \boldsymbol{p}_e}{\partial q_i} \dot{q}_i = \sum_{i=1}^{n} \boldsymbol{J}_{Pi} \dot{q}_i \qquad (43)$$

This expression shows how $\dot{\boldsymbol{p}}_e$ can be obtained as the sum of the terms $\dot{q}_i \boldsymbol{J}_{Pi}$. Each term represents the contribution of the velocity of single Joint *i* to the end-effector linear velocity when all the other joints are still.
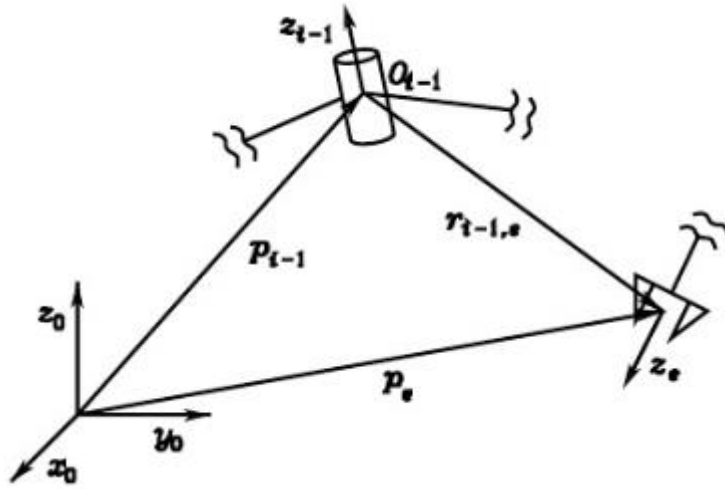
*Figure. 13- Representation of a vectors needed for the computation of the velocity contribution of a revolute joint to the end-effector linear velocity [9].*

In the case of *revolute* Joint ($q_i = \vartheta_i$), observing that the contribution to the linear velocity is to be computed with reference to the origin of the end-effector frame (Figure 13), it is

$$\dot{q}_i \boldsymbol{J}_{Pi} = \boldsymbol{\omega}_{i-1,i} \times \boldsymbol{r}_{i-1,e} = \dot{\vartheta}_i \boldsymbol{z}_{i-1} \times (\boldsymbol{p}_e - \boldsymbol{p}_{i-1}) \tag{44}$$

and then

$$\boldsymbol{J}_{Pi} = \boldsymbol{z}_{i-1} \times (\boldsymbol{p}_e - \boldsymbol{p}_{i-1}). \tag{45}$$

For the contribution to the *angular velocity*, in view of (39), it is

$$\boldsymbol{\omega}_e = \boldsymbol{\omega}_n = \sum_{i-1}^{n} \boldsymbol{\omega}_{i-1,i} = \sum_{i-1}^{n} \boldsymbol{J}_{oi} \dot{q}_i, \tag{46}$$

where (40) has been utilized to characterize the terms $\dot{q}_i \boldsymbol{J}_{oi}$, and thus in detail, from (40) it is

$$\dot{q}_i \boldsymbol{J}_{oi} = \dot{\vartheta}_i \boldsymbol{z}_{i-1} \tag{47}$$

and then

$$\boldsymbol{J}_{oi} = \boldsymbol{z}_{i-1} \tag{48}$$

In summary, the Jacobian in (15) can be portioned into the $(3\times 1)$ column vectors $\boldsymbol{J}_{Pi}$ and $\boldsymbol{J}_{Oi}$ as

$$\boldsymbol{J} = \begin{bmatrix} \boldsymbol{J}_{P1} & & \boldsymbol{J}_{Pn} \\ & \cdots & \\ \boldsymbol{J}_{O1} & & \boldsymbol{J}_{On} \end{bmatrix}, \tag{49}$$

where

$$\begin{bmatrix} \boldsymbol{J}_{Pi} \\ \boldsymbol{J}_{Oi} \end{bmatrix} = \begin{bmatrix} \boldsymbol{z}_{i-1} \times (\boldsymbol{p}_e - \boldsymbol{p}_{i-1}) \\ \boldsymbol{z}_{i-1} \end{bmatrix} \text{ for a } revolute \text{ joint.} \tag{50}$$

The expressions in (50) allow Jacobian computation in a simple, systematic way on the basis of direct kinematics relations. In fact, the vectors $\boldsymbol{z}_{i-1}, \boldsymbol{p}_e$ and $\boldsymbol{p}_{i-1}$ are all functions of the joint variables. In particular:

- $\boldsymbol{z}_{i-1}$ is given by the third column of the rotation matrix $\boldsymbol{R}_{i-1}^0$,

$$\boldsymbol{z}_{i-1} = \boldsymbol{R}_1^0 \dots \boldsymbol{R}_{i-1}^{i-2}(q_{i-1})\boldsymbol{z}_0 \tag{51}$$

where $\boldsymbol{z}_0 = \begin{bmatrix} 0 & 0 & 1 \end{bmatrix}^T$ allows the selection of the third column.

- $\boldsymbol{p}_e$ is given by the first three elements of the fourth column of the transformation matrix $\boldsymbol{T}_e^0$, by expressing $\widetilde{\boldsymbol{p}}_e$ in the $(4\times 1)$ homogeneous form

$$\widetilde{\boldsymbol{p}}_e = \boldsymbol{A}_1^0(q_1) \dots \boldsymbol{A}_n^{n-1}(q_n)\widetilde{\boldsymbol{p}}_0 \tag{52}$$

where $\widetilde{\boldsymbol{p}}_0 = \begin{bmatrix} 0 & 0 & 0 & 1 \end{bmatrix}^T$ allows the selection of the fourth column.

- $\boldsymbol{p}_{i-1}$ is given by first three elements of the fourth column of the transformation matrix $\boldsymbol{T}_{i-1}^0$, it can be extracted from

$$\widetilde{\boldsymbol{p}}_{i-1} = \boldsymbol{A}_1^0(q_1) \dots \boldsymbol{A}_{i-1}^{i-2}(q_{i-1})\widetilde{\boldsymbol{p}}_0. \tag{53}$$

The above equations can be conveniently used to compute the translational and rotational velocities of any point along the manipulator structure, as long as the direct kinematics functions relative to that point are known. Finally, notice that the Jacobian matrix depends on the frame in which the end-effector velocity is expressed. The above equations allows

computation of the geometric Jacobian with respect to the base frame. If it is desired to represent the Jacobian in a different Frame $u$, it is sufficient to know the relative rotation $R^u$. The relationship between velocities in the two frames is

$$\begin{bmatrix} \dot{p}_e^u \\ \dot{\omega}_e^u \end{bmatrix} = \begin{bmatrix} R^u & O \\ O & R^u \end{bmatrix} \begin{bmatrix} \dot{p}_e \\ \dot{\omega}_e \end{bmatrix}, \tag{54}$$

Which, substituted in (14), gives

$$\begin{bmatrix} \dot{p}_e^u \\ \dot{\omega}_e^u \end{bmatrix} = \begin{bmatrix} R^u & O \\ O & R^u \end{bmatrix} J\dot{q}, \tag{55}$$

and then

$$J^u = \begin{bmatrix} R^u & O \\ O & R^u \end{bmatrix} J, \tag{56}$$

Where $J^u$ denotes the geometric Jacobian in a Frame $u$, which has been assumed to be time-invariant.

$$\begin{bmatrix} \dot{p}_e^u \\ \dot{\omega}_e^u \end{bmatrix} = J^u \dot{q} \tag{57}$$

### 2.2.3.2 Statics

The goal of statics is to determine the relationship between the generalized forces applied to the end-effector and the generalized forces applied to the joints – torques for revolute joints- with the manipulator at an equilibrium configuration.

Let $\tau$ denote the ($n \times 1$) vector of joint torques and $\gamma$ the ($r \times 1$) vector of end-effector forces where $r$ is the dimension of the operational space of interest.

The application of the *principle of virtual work* allows the determination of the required relationship. The mechanical manipulators considered are systems with time-invariant, holonomic constraints, and thus their configurations depend only on the joint variables $\mathbf{q}$ and not explicitly on time. This implies that virtual displacements coincide with elementary displacements. Consider the elementary works performed by the two force systems. As for the joint torques, the elementary work associated with them is

$$dW_\tau = \boldsymbol{\tau}^T d\boldsymbol{q}. \tag{58}$$

As for the end-effector forces $\boldsymbol{\gamma}$, if the force contributions $\boldsymbol{f}_e$ are separated by the moment contributions $\boldsymbol{\mu}_e$, the elementary work associated with them is

$$dW_\gamma = \boldsymbol{f}_e^T d\boldsymbol{p}_e + \boldsymbol{\mu}_e^T \boldsymbol{\omega}_e dt, \tag{59}$$

where $d\boldsymbol{p}_e$ is the linear displacement and $\boldsymbol{\omega}_e dt$ is the angular displacement. By accounting for the differential kinematics relationship in (14),(15), the relation (59) can be rewritten as

$$dW_\gamma = \boldsymbol{f}_e^T \boldsymbol{J}_P(\boldsymbol{q})d\boldsymbol{q} + \boldsymbol{\mu}_e^T \boldsymbol{J}_O(\boldsymbol{q})d\boldsymbol{q} = \gamma_e^T \boldsymbol{J}(\boldsymbol{q})d\boldsymbol{q} \tag{60}$$

where $\gamma_e = [\boldsymbol{f}_e^T \quad \boldsymbol{\mu}_e^T]^T$. Since virtual and elementary displacements coincide, the virtual works associated with the two force systems are

$$dW_\tau = \boldsymbol{\tau}^T \delta\boldsymbol{q} \tag{61}$$

$$dW_\gamma = \gamma_e^T \boldsymbol{J}(\boldsymbol{q})\delta\boldsymbol{q}, \tag{62}$$

Where $\delta$ is the usual symbol to indicate virtual quantities.

According to the principle of virtual work, the manipulator is a *static equilibrium* if and only if

$$dW_\tau = dW_\gamma \qquad \forall \delta\boldsymbol{q}, \tag{63}$$

the difference between the virtual work of the joint torques and the virtual work of the end-effector forces must be null for all joint displacements.

From (62), notice that the virtual work of the end-effector forces is null for any displacement in the null space of **J**. This implies that the joint torques associated with such displacements must be null at static equilibrium. Substituting (61),(62) into (63) leads to the notable result

$$\boldsymbol{\tau} = \boldsymbol{J}^T(q)\boldsymbol{\gamma}_e \qquad\qquad (64)$$

Stating that the relationship between the end-effector forces and the joint torques is established by the transpose of the manipulator geometric Jacobian.

# 3 State of art-Principles of stiffness estimation

The robot is able to accommodate the forces applied to an endpoint with acceptable displacements and, with the appropriate stiffness. In this chapter, we introduce the fundamental concepts and properties of a stiffness manipulator arm and we will be analyzing all the possible methods, both experimental and theoretical, that allow the assessment the stiffness of the joints .

## 3.1 Basic methodology

The theoretical approach appears easily applicable and it leads to reliable results only if the degree of freedom of manipulator analyzed is reduced (Degrees of freedom $\leq$ 2). In fact the first example that is listed is a manipulator with 2-Dof. In this case, it is possible to determine the displacements of end-effector in addition to joint stiffness, with an eigenvalue problem.

When number of degrees of freedom increase, the estimation of stiffness joints is becoming increasingly difficult, therefore it is necessary to verify the results obtained from the theoretical approach with experimental test.

There are several sources that produce deflections of a manipulators arm. Arm links, for example, may deflect when a large force is applied. In particular, when the arm length gets longer, as for example in the space shuttle manipulator, the deflection resulting from the links compliance is the major source of the endpoint deflection.

In the majority of today's industrial robots, however, the major deflection occurs in joints, each joint is driven by an individual actuator through a reducer and transmission mechanisms.

When a drive force or torque is transmitted, each member involved may deflect. Also, the actuator itself has a limited stiffness determined by its feedback control system, which generates the drive torque based on the discrepancy between the reference position and the actual measured position.

As we mentioned earlier, the robot deflection is depends on its link and joint flexibilities, although the joint flexibilities are mainly responsible for the global flexibility Accordingly, in order to come up with a simple stiffness model of the robot, it is assumed that its link are

rigid and its joints are linear elastic torsional springs. The damping is also supposed to be negligible for a matter of a model simplicity. The stiffness of the drive system combined with the stiffness of the reducer and transmissions can be considered as a spring constant $k_i$ that relates the deflection at joint $i$ to force or torque transmitted. Namely,

$$\tau_i = k_i \Delta q_i \tag{65}$$

Where $\tau_i$ is the joint torque and $\Delta q_i$ is the deflection at joint axis.

In the following analysis, we assume that the arm links are rigid and we investigated the end point stiffness based on the model of the joint stiffness given by (65).
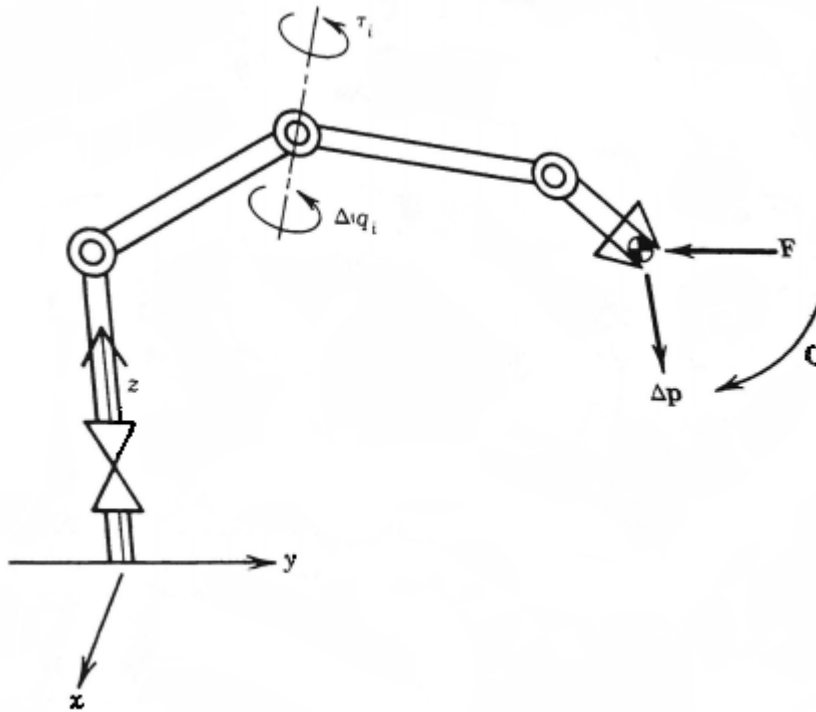


*Figure 14- Endpoint compliance and joint servo stiffness [12].*

### 3.1.1  Endpoint compliance analysis

We derived the endpoint stiffness from the individual joint stiffness. As shown in Figure 14, we derived the endpoint and moment by the m-dimensional vector $\vec{F}$ and the resultant deflection by $\Delta p$, both of them defined  with reference to the base coordinate frame. When we neglect gravity and friction at the joints, the endpoint force can be converted to the equivalent joint torques according to the theorem, namely, the equation (64).

Where $\boldsymbol{J}^T$ is the *nxm* transpose of the manipulator Jacobian, it is referred to end-effector. At the individual joints, joint torques $\boldsymbol{\tau}$ *(nx1)* are related to joint deflections $\Delta \boldsymbol{q}$ by the individual stiffness as we modeled in the previous section. For convenience, let us rewrite (65) in the vector form:

$$\boldsymbol{\tau} = \boldsymbol{K}\Delta \boldsymbol{q} \tag{66}$$

Where **K** is a *nxn* diagonal matrix given by

$$\boldsymbol{K} = \begin{bmatrix} k_1 & & 0 \\ & \ddots & \\ 0 & & k_n \end{bmatrix} \tag{67}$$

The individual joint deflections $\Delta \boldsymbol{q}$ produce the endpoint deflection $\Delta p$ according to

$$\Delta \boldsymbol{p} = \boldsymbol{J}\Delta \boldsymbol{q} \tag{68}$$

When the individual joint drive systems are active and the stiffnesses are no-zero, the matrix **K** is invertible.

Substituting (64) and(66) into (68), we obtain:

$$\Delta \boldsymbol{p} = \boldsymbol{C}\boldsymbol{\gamma}_e \tag{69}$$

Where

$$\boldsymbol{C} = \boldsymbol{J}\boldsymbol{K}^{-1}\boldsymbol{J}^T \tag{69.a}$$

Thus the deflection at the endpoint $\Delta \boldsymbol{p}$ is related to the endpoint force $\boldsymbol{\gamma}_e$ by the *mxm* matrix **C**.

The matrix $\mathbf{C}$ is called the compliance matrix of the arm endpoint. The compliance matrix is invertible if the manipulator Jacobian is a square matrix and of full rank:

$$\boldsymbol{\gamma}_e = \boldsymbol{C}^{-1}\Delta\boldsymbol{p} \tag{70}$$

the inverse of the compliance matrix is called the stiffness matrix of the arm endpoint.

When the manipulator Jacobian is degenerate, the stiffness becomes infinite in at least one direction.

The endpoint compliance matrix and the stiffness matrix consist of the individual joint stiffness and manipulator Jacobian.

Since the Jacobian varies with the arm configuration, the compliance matrix is configuration dependent. Also, at a given arm configuration, the magnitude of the endpoint deflection varies with the direction of the endpoint force.

### 3.1.2 The principal transformation of compliance matrices

As mentioned in the previous section, the endpoint deflection of a manipulator's arm depend not only on the arm configuration but also on the direction of the applied endpoint force.

In this section, we analyze the maximum and minimum deflections of the arm's endpoint and characterize the compliance matrix. To simplify the analysis we deal with two DOF planar manipulator show in figure:
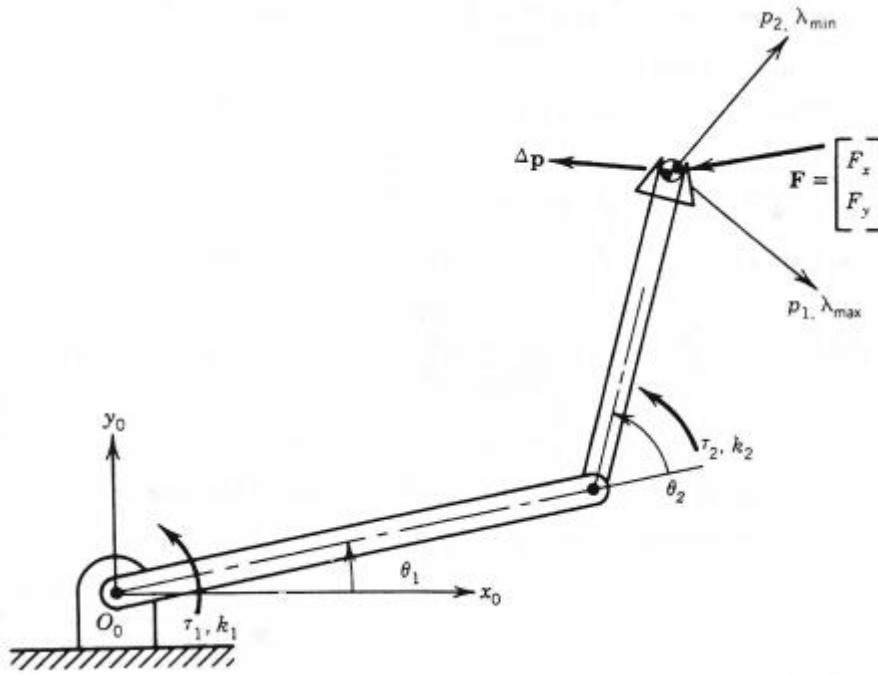
*Figure 85 – Principal directions of endpoint compliance[12].*

The endpoint deflection and the endpoint force are represented by the two-dimensional vectors $\Delta \boldsymbol{p} = [\Delta x, \Delta y]^T$ and the $\boldsymbol{\gamma}_e = [F_x, F_y]^T$, respectively. We begin with deriving the endpoint compliance matrix from equation ($\boldsymbol{C} = \boldsymbol{J}\boldsymbol{K}^{-1}\boldsymbol{J}^T$) namely,

$$\begin{bmatrix} \dfrac{(l_1 s_1 + l_2 s_{12})^2}{k_1} + \dfrac{l_2^2 s_{12}^2}{k_2} & -\dfrac{(l_1 c_1 + l_2 c_{12})(l_1 s_1 + l_2 s_{12})}{k_1} - \dfrac{l_2^2 c_{12} s_{12}}{k_2} \\ -\dfrac{(l_1 c_1 + l_2 c_{12})(l_1 s_1 + l_2 s_{12})}{k_1} - \dfrac{l_2^2 c_{12} s_{12}}{k_2} & \dfrac{(l_1 c_1 + l_2 c_{12})^2}{k_1} + \dfrac{l_2^2 c_{12}^2}{k_2} \end{bmatrix} \quad (71)$$

Equations (67) and (69.a) imply that the compliance matrix is always symmetric, and it can be verified in equation (71). We search the maximum and minimum deflections and their directions when a unit magnitude force is applied to the endpoint for the compliance matrix obtained above and for a given arm configuration. From (69) the squared norm of the endpoint deflection is given by

$$|\Delta \boldsymbol{p}|^2 = \Delta \boldsymbol{p}^T \Delta \boldsymbol{p} = \boldsymbol{\gamma}_e^T \boldsymbol{C}^T \boldsymbol{C} \boldsymbol{\gamma}_e = \boldsymbol{\gamma}_e^T \boldsymbol{C}^2 \boldsymbol{\gamma}_e \quad (72)$$

Where **C** is symmetric. We evaluate the maximum and minimum deflection under the condition on the magnitude of the endpoint force:

$$|\boldsymbol{\gamma}_e|^2 = \boldsymbol{\gamma}_e{}^T \boldsymbol{\gamma}_e = 1 \tag{73}$$

To solve this problem, we employ Lagrange multiplier $\lambda$ to define:

$$L = \boldsymbol{\gamma}_e{}^T \boldsymbol{C}^2 \boldsymbol{\gamma}_e - \lambda(\boldsymbol{\gamma}_e{}^T \boldsymbol{\gamma}_e - 1) \tag{74}$$

The necessary condition for the squared norm of the endpoint deflection to take extreme values is given by:

$$\frac{\partial L}{\partial \lambda} = 0, \qquad \boldsymbol{\gamma}_e{}^T \boldsymbol{\gamma}_e - 1 = 0 \tag{75}$$

Which is identical to (73) and

$$\frac{\partial L}{\partial F} = 0, \qquad \boldsymbol{C}^2 \boldsymbol{\gamma}_e - \lambda \boldsymbol{\gamma}_e = 0 \tag{76}$$

From equation (76), it follows that the Lagrange multiplier is the eigenvalue of the squared compliance matrix $\boldsymbol{C}^2$. Thus the problem of finding the maximum and minimum deflections is basically an eigenvalue problem.

Solving the characteristic equation for $\boldsymbol{C}^2$ yields the maximum and minimum eigenvalues

$$\begin{matrix} \lambda_{max} \\ \lambda_{min} \end{matrix} = \frac{1}{2}[a_1 + a_2 \pm \sqrt{(a_1 - a_2)^2 + 4a_2^3}] \tag{77}$$

where

$$\boldsymbol{C}^2 = \begin{bmatrix} a_1 & a_3 \\ a_3 & a_2 \end{bmatrix} \tag{78}$$

Since the individual joint stiffness are positive, both eigenvalues are positive Using the eigenvalues and equations (75) and (76), the squared norm of the endpoint deflection is given by

$$|\Delta \boldsymbol{p}|^2 = \boldsymbol{\gamma}_e{}^T \boldsymbol{C}^2 \boldsymbol{\gamma}_e = \boldsymbol{\gamma}_e{}^T \lambda \boldsymbol{\gamma}_e = \lambda \tag{79}$$

Thus, the maximum and minimum deflections are given by $\sqrt{\lambda_{max}}$ and $\sqrt{\lambda_{min}}$, respectively.

The direction in which the maximum or minimum deflection occurs is given by the eigenvector corresponding to the maximum or minimum eigenvalue.

Figure 15 illustrates the directions of eigenvectors. Note that the two directions are orthogonal to each other.

These directions are referred as principal directions. Coordinate axes are defined in the principal directions and we consider them as principal axes. The compliance matrix becomes diagonal when expressed in the principal coordinates.

If we consider $e_1$ and $e_2$ as unit vectors along the principal axes, associated respectively with the maximum and minimum eigenvalue; and if E is a 2x2 matrix consisting of $e_1$ and $e_2$:

$$E = [e_1 \ e_2] \tag{80}$$

The compliance matrix is transformed to the diagonal zed form $C^*$ in the principal coordinates:

$$C^* = E^T C E = \begin{bmatrix} \sqrt{\lambda_{max}} & 0 \\ 0 & \sqrt{\lambda_{min}} \end{bmatrix} \tag{81}$$

where $E^T = E^{-1}$ since E is orthonormal.

The coordinate transformation of the principal coordinates is referred as the principal transformation. When the endpoint force is applied in the principal direction, the deflection occurs in the same principal direction and the magnitude of the deflection has extreme value.

## 3.2 State-of-art methodology and other methods for stiffness evaluation

In the previous paragraph, a method for an estimation of stiffness for a manipulator with two degrees of freedom was submitted The method presents the principal theoretical basis on which methods for stiffness determination are presented.

In this paragraph some methods of stiffness estimation will be shown, showing an explication of issues which emerg when the articulations increase.

The first method consists of clamping all the joints except one to measure its stiffness and repeating the procedure for each joint. For example in the UR5, the clamping of articulations is realized using a break, shown in the figure below:



*Figure 16- UR5 break[13]*
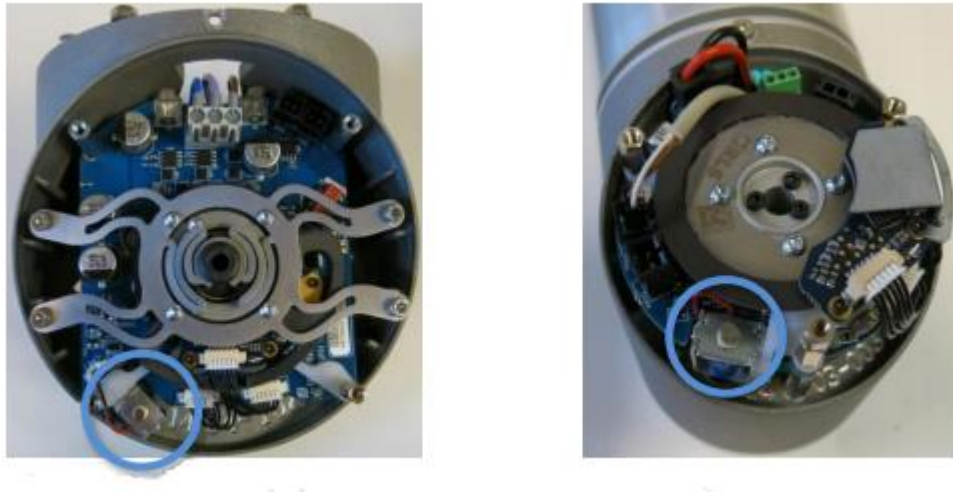
If the stiffness link are known, to obtain the results of the Cartesian stiffness matrix (CaSM) of the robot through its Cartesian workspace, it is enough to execute a number of experiments equal to number of joints. CaSM is a matrix defined as follows:

$$\gamma_e = K_X \delta d \qquad (82)$$

In the case of UR5 with only six measurements to obtain the value of Cartesian stiffness matrix.

However, to block the joints is not an easy task and the stiffness links are not usually known. The second method consists of measuring the deflection of the robot caused by some loads exerted on its end-effector and evaluating its stiffness throughout its Cartesian workspace by through interpolations. This method provides better results, but many configurations have to be tested in order to get a good approximation of the CaSM of the robot throughout its Cartesian workspace. This two method were presented in [14]

Below it is shown the method adopted for the evaluation of stiffness joints. In this work the robotic-system responses to applied external wrench under static equilibrium is analyzed through the CaSM of the robot. It is possible to determine the translation and angular deflections of the robot EE when it is subjected to an applied wrench.

Before beginning, it is given an introduction of stiffness modelling. The formula $(64)$[1] can also be expressed as a function of $\delta\boldsymbol{\theta}$, the $n$-dimensional vector of variations in the joint angles, as follows:

$$\boldsymbol{\tau} = \boldsymbol{K}_\theta \delta\boldsymbol{\theta} \tag{83}$$

with

$$\boldsymbol{K}_\theta = \begin{bmatrix} k_{\theta_1} & 0 & 0 & 0 & 0 \\ 0 & k_{\theta_2} & 0 & 0 & 0 \\ 0 & 0 & \ddots & 0 & 0 \\ 0 & 0 & 0 & k_{\theta_{n-1}} & 0 \\ 0 & 0 & 0 & 0 & k_{\theta_n} \end{bmatrix} \tag{85}$$

The differentiation of (64) with respect to $\boldsymbol{\theta}$ and considering finite increments of time leads to the following relationship:

$$\frac{\partial\boldsymbol{\tau}}{\partial\theta} = \left(\frac{\partial\boldsymbol{J}^T}{\partial\theta}\right)\boldsymbol{\gamma}_e + \boldsymbol{J}^T \frac{\partial\boldsymbol{\gamma}_e}{\partial\boldsymbol{d}}\frac{\partial\boldsymbol{d}}{\partial\theta} \tag{86}$$

moreover, as defined previously:

---

[1] In the Equation 64, it is shown below., the Jacobian is referred to end-effector:

$$\boldsymbol{\tau} = \boldsymbol{J}^T(q)\boldsymbol{\gamma}_e$$

$$\gamma_e = K_X \delta d \qquad (87)$$

where $K_X$ is the Cartesian stiffness matrix and $\delta d$ the $n$-dimensional small displacement of the robot end-effector .

From Equations (83) and (87) and also the Equation (14),we obtain the following expression:[2]

$$K_\theta = K_C + J^T K_X J \qquad (88)$$

with

$$K_C = \left[ \frac{\partial J^T}{\partial \theta_1} \gamma_e \quad \frac{\partial J^T}{\partial \theta_2} \gamma_e \quad \cdots \quad \frac{\partial J^T}{\partial \theta_{n-1}} \gamma_e \quad \frac{\partial J^T}{\partial \theta_n} \gamma_e \right] \qquad (89)$$

being the complementary stiffness matrix $K_C$ defined in [15] , physically $K_C$ give us an information of variance of Jacobian, that is due to application of load.

That amounts to

$$K_X = J^{-T}(K_\theta - K_C)J^{-1} \qquad (90)$$

By introducing the stiffness modeling, we can see a method proposed for the joint stiffness identification, illustrated in the following figure (Figure 17) :

---

[2]

Equation 14

$$v = \begin{bmatrix} \dot{p} \\ \omega \end{bmatrix} = J(q) \, \dot{q}$$

where the $\dot{q} = [\dot{\theta}_1, \ldots, \dot{\theta}_n]^T$ and $v = [\frac{\partial x}{\partial t}, \frac{\partial y}{\partial t}, \frac{\partial z}{\partial t}, \frac{\partial \alpha}{\partial t}, \frac{\partial \beta}{\partial t}, \frac{\partial \gamma}{\partial t}]^T$
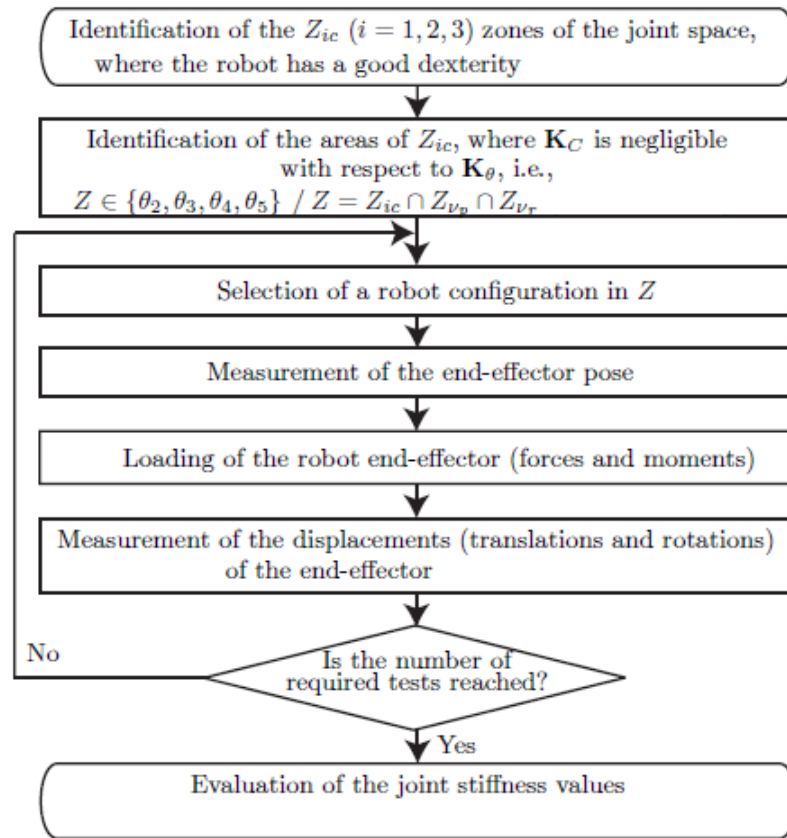
*Figure 17 - Procedure for the joint stiffness identification[16].*

First, the zones of the robot workspace and joint space in which the robot has a good dexterity[3] are identified. Following simplification allows to choose the configurations in the good dexterity zones:

---

[3] It is said that a robot has a good dexterity when the workspace zones are easily reachable and avoid self-collisions with itself. Indeed the robot dexterity changes in the workspace. In the figure below is shown the workspace dexterity of a KUKA-DLR LBR arm:
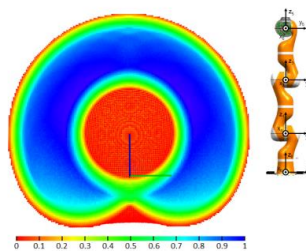


Dexterity of KUKA-DLR LBR arm[17]

$$K_X = J^{-T}K_\theta J^{-1} \tag{91}$$

It appears that a good dexterity is required for a good convergence of the procedure. Then, the areas in which $K_C$ is negligible with respect to $K_\theta$ are identified as the stiffness model of the robot can be simplified in those areas. Once good robot configurations are obtained, some of them can be selected in order to perform some tests.

### 3.2.1  Optimal robot configurations according to kinematic performance

From (90), it makes sense that the numerical determination of the joint stiffness values is highly sensitive to the conditioning number of **J** [4]; Indeed, matrices with condition numbers out of certain restraints are termed ill-conditioned because of this undesired behavior. Optimally-conditioned matrices are those with a condition number of unity or also near the unit, and are called isotropic. The worst-conditioned are singular matrices, with a condition number of infinity. As a consequence, the conditioning number of Jacobian matrix is used as a criterion to select appropriate robot configurations for the tests and it is used to measure the robot dexterity.

For knowing the condition number of a matrix is reported a method based on the Frobenius norm. The computation of Frobenius norm requires only the inversion of a positive-definite 6x6 matrix, as can been seen in the footnote [19][5]. However, it may happen that

---

blue indicates areas with higher dexterity of the manipulator. For a more detailed discussion of dexterity are given the following references [17][18]:

[4]

The conditioning number gives an indication on the accuracy of the results obtained by solving the linear system by inversion of the matrix. Values close to 1 of the conditioning number indicate that the array is well conditioned.

[5] The *condition number* $k_F(M)$ of a $m \times n$ matrix **M**, with $m \le n$, is defined as follows:

$$k_F(\mathbf{M}) = \frac{1}{m}\sqrt{tr(\mathbf{M}^T\mathbf{M})tr[(\mathbf{M}^T\mathbf{M})^{-1}]} \tag{92}$$

This provides an analytical expression of the condition number depending on the posture parameters.

the terms of matrix **J** are not homogeneous, because in the matrix different units of measurement are present In fact, from Equations (49) and (50) it is apparent that the columns of **J** are not dimensionally homogeneous, as the unit vectors $z_{i-1}$ are dimensionless, while vectors $z_{i-1} \times (p_e - p_{i-1})$ have units of length. Therefore, the result would be meaningless for the condition number of matrix **J**. In this case the Jacobian can be normalized by means of a *normalizing length[6]*, in following a way:

$$J_N = \begin{bmatrix} \frac{1}{L}I_{3x3} & 0_{3x3} \\ 0_{3x3} & I_{3x3} \end{bmatrix} J \qquad (93)$$

where $0_{3x3}$ is the 3x3 zero matrix and $I_{3x3}$ is the 3x3 identity matrix.

It is noteworthy here that the condition number is computed only to identify the zones where the robot has a good dexterity. It appears that the condition number of the normalized Jacobian ($J_N$) depends on the characteristic length L, used to normalization , but not the location of the zones.

$$k_F(J_N) = \frac{1}{m} \sqrt{tr(J_N{}^T J_N) tr\left[(J_N{}^T J_N)^{-1}\right]} \qquad (94)$$

The choice of appropriate robot configurations for the identification of the joint stiffness values is made by choosing the zones of workspace where the value of the inverse condition number of $J_N$ is higher. Therefore, the iso-contours of the inverse condition number of $J_N$ based on the Frobenius norm can be depicted throughout the robot Cartesian workspace. An example of isocontours is given below :

---

[6] The explanation of *normalizing length* and a its geometric interpretation is given in the paragraph 3.2.1.1
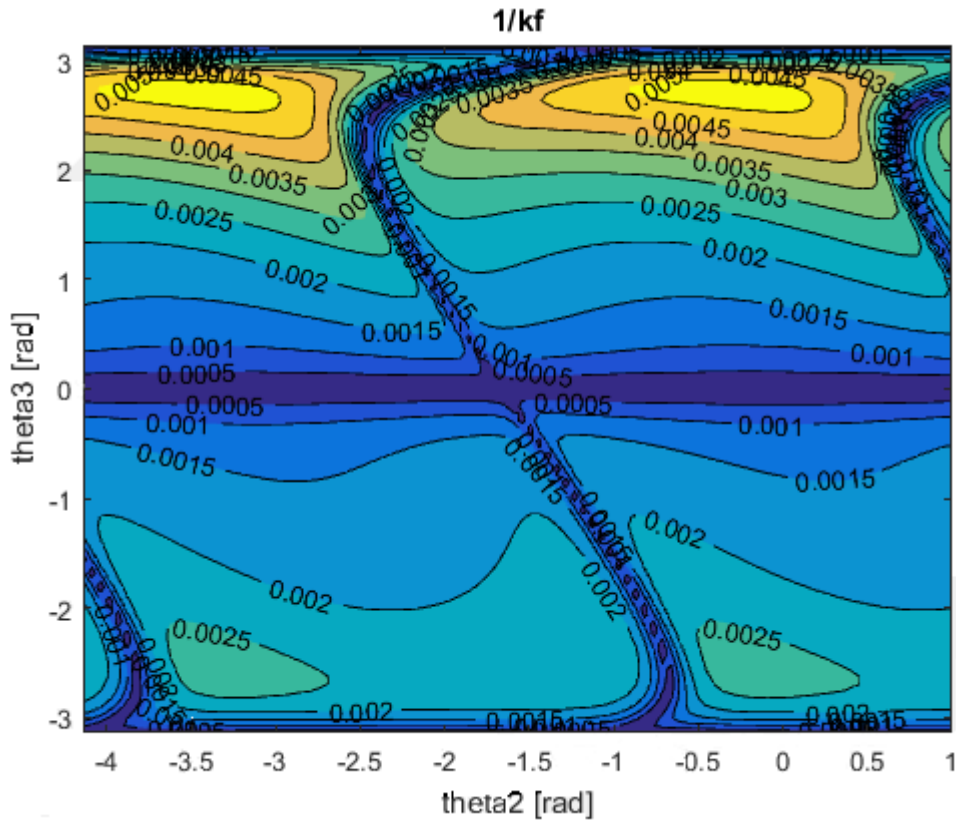
*Figure 98- Iso-contour example*

The higher $k_F(J_N)^{-1}$, the better the dexterity. On the contrary, with lower $k_F(J_N)^{-1}$, the is getting closer to the singularities.

The joint stiffness values are determined from (90); given that we have proposed the hypothesis that $K_C$ is negligible with respect to $K_\theta$, the equation (90) is reduced to the following equation :

$$K_X \approx J^{-T}K_\theta J^{-1} \tag{95}$$

From this analysis, it follows from that the robot configurations for which the influence of $K_C$ on $K_X$ are at their maximum are also those for which $k_F(J_N)^{-1}$ is at its minimum, close to singularity.

### 2.2.3.3 Normalizing length

The numerical conditioning of the Jacobian matrix plays a crucial role for investigating the kinetostatic performance of a manipulator.

If in Equations (14) and (64) $\mathbf{J}$ has a large condition number, it may cause large changes in the computed values of $\boldsymbol{\tau}$ and $\boldsymbol{q}$. Matrices with condition numbers above a certain allowable bound are termed ill-conditioned because of this undesired behavior. Optimally-conditioned matrices, on the other hand, are those with a condition number of unity, and are called isotropic[7]. The worst-conditioned are singular matrices, with a condition number of infinity. As noted above, A measure of the numerical conditioning of matrices is the condition number .

However from Equations (49) and (50) it is apparent that the columns of $\mathbf{J}$ are not dimensionally homogeneous. This dimensional inhomogeneity gives rise to inconsistencies when evaluating the condition number under discussion, for it prevents us from ordering the singular values of the Jacobian matrix from smallest to largest. We circumvent this problem by performing a normalization of the entries of the Jacobian matrix, by dividing the firsts three rows of $\mathbf{J}$ by a normalizing length obtaining $\boldsymbol{J_N}$.

$$\boldsymbol{J_N J_N^T} = \sigma \boldsymbol{I}_m \tag{96}$$

The isotropic condition for the normalized Jacobian matrix is, for instance $m=6$, then:

$$\boldsymbol{J_N J_N^T} = \sigma \boldsymbol{I}_6 \tag{97}$$

If $\boldsymbol{J_N}$ is isotropic the lower-right block in Equation (97) is:

$$\sum_1^n \boldsymbol{z}_i \boldsymbol{z}_i^T = \sigma \boldsymbol{I}_3 \tag{98}$$

Upon equating the trace of both sides of the above equation, we obtain

---

[7] A matrix is isotropic if all its singular values are identical and nonzero. This is equivalent to saying that, if $\mathbf{M}$ is isotropic, where $\mathbf{M}$ is a generic matrix *mxm*, then a real number σ exists such that:

$$\boldsymbol{MM^T} = \sigma \boldsymbol{I}_m$$

where $\sigma$ is the common singular value of $\mathbf{M}$ and $\boldsymbol{I}_m$ is the *mxm* identity matrix

$$n = 3\sigma^2 \tag{99}$$

Moreover using the upper-left block in Equation (96), solving for L we can obtain:

$$\frac{1}{L^2} \sum_1^n \|z_i \times (p_e - p_i)\| = 3\sigma^2 \tag{100}$$

with the Equation (98), substituting in the (99), we obtain:

$$L^2 = \frac{\sum_1^n \|z_i \times (p_e - p_i)\|}{n} \tag{101}$$

In the foregoing expression, we can see a geometric interpretation of the characteristic length, L, L is the root-mean squared (RMS) value of the distances of the $n$ joint axes to the operation point of the end-effector at the isotropic posture of the manipulator, where a manipulator is called isotropic if it can attain a set of configurations in its workspace at which the Jacobian matrix is isotropic[20] .

In this work, the characteristic length L calculates as follows. Firstly the maximum reach $\bar{R}$ is calculate, which represents the maximum distance of the operation point, end-effector, from the first revolute axis, where the invariant frame is placed. Certain simplifications can be made, for example, the first joint variable has no influence on this reach, because it produces rigid body motions of the overall manipulator, and thus leave the frame-invariant condition number unchanged, and therefore, can be locked at an arbitrary value of 0. The problem consists in maximizing the distance, as explained above, over the remaining joint variables:

$$\max_\theta \|p_e - p_0\| \tag{102}$$

where:

$$\theta = [\theta_2, \theta_3, \dots, \theta_n]^T \tag{103}$$

The maximum reach is $\bar{R} = \max_\theta \|p_e - p_0\|$. Besides, for the convexity [21] of the Euclidean norm the found maximum is global. In the end, if a reach is denoted by R, then the robot characteristic length L is:

$$L = \frac{R}{\bar{R}} \tag{104}$$

For instance in the case study of this work, the UR5 reach is 850 mm.

### 3.2.2   Evaluation of the joint stiffness

From equation (95) and assuming that $\boldsymbol{K}_C$ is negligible with respect to $\boldsymbol{K}_\theta$ thanks to an appropriate robot configuration, the equation (87) can be rewritten as

$$\boldsymbol{\gamma}_e = \boldsymbol{J}^{-T}\boldsymbol{K}_\theta\boldsymbol{J}^{-1}\delta\boldsymbol{d} \tag{105}$$

Hence, the $n$-dimensional robot end-effector displacement vector $\delta\boldsymbol{d}$ takes form

$$\delta\boldsymbol{d} = \boldsymbol{J}\boldsymbol{K}_\theta^{-1}\boldsymbol{J}^T\boldsymbol{\gamma}_e \tag{106}$$

Let the joint compliances be the components of the $n\times 1$ vector $\mathbf{x}$, namely,

$$\mathbf{x} = \begin{bmatrix} 1/k_{\theta_1} & 1/k_{\theta_2} & \cdots & 1/k_{\theta_{n-1}} & 1/k_{\theta_n} \end{bmatrix}^T \tag{107}$$

From equation (106), it turns out that

$$\delta\boldsymbol{d} = \begin{bmatrix} \sum_{j=1}^{n}\left(x_j J_{1j}\sum_{i=1}^{n}J_{ij}\gamma_{e_i}\right) \\ \vdots \\ \sum_{j=1}^{n}\left(x_j J_{nj}\sum_{i=1}^{n}J_{ij}\gamma_{e_i}\right) \end{bmatrix} \tag{108}$$

$x_j$ begin the $j$th component of vector $\mathbf{x}$, $x_j = 1/k_{\theta_j}$ $j = 1, \dots, \text{n}, ,$ and $\gamma_{e_i}$ being the $j$th

component of vector $\boldsymbol{\gamma}_e$.

By isolating the components of vector $\mathbf{x}$ in equation (108), the joint compliances can be expressed with respect to the robot end-effector displacements as follows:

$$\boldsymbol{A}\boldsymbol{x} = \delta\boldsymbol{d} \tag{109}$$

$\mathbf{A}$ is a $n \times n$ matrix taking the form

$$A = \begin{bmatrix} J_{11} \sum_{i=1}^{n} J_{i1}\gamma_{e_i} & \cdots & J_{1n} \sum_{i=1}^{n} J_{in}\gamma_{e_i} \\ \vdots & \ddots & \vdots \\ J_{n1} \sum_{i=1}^{n} J_{i1}\gamma_{e_i} & \cdots & J_{nn} \sum_{i=1}^{n} J_{in}\gamma_{e_i} \end{bmatrix} \qquad (110)$$

It is noteworthy that a 6-dimensional wrench vector, a 6-dimensional end-effector displacement vector and a $n \times n$ $A$ matrix are associated with each test. Let $B_i$ and $c_i$ be the matrix $A$ and the small displacement screw $\delta d$ corresponding to the $i$th test, respectively. Assuming that n test(s) are used to find $x$, we obtain:

$$Bx = c \qquad (111)$$

with

$$B = \begin{bmatrix} B_1 \\ \vdots \\ B_i \\ \vdots \\ B_n \end{bmatrix} \qquad (112)$$

and

$$c = \begin{bmatrix} c_1 \\ \vdots \\ c_i \\ \vdots \\ c_n \end{bmatrix} \qquad (113)$$

It should be noted that the linear-equation system (111)becomes overdetermined when $n>1$ as matrix $B$ is no longer square, but rectangular. In that case, the joint stiffness values are obtained by minimizing the Euclidean norm of the approximation error of the overdetermined linear-equation system (111), namely,

$$\text{minimize } e(x) \equiv \frac{1}{2}\|Bx - c\|_2^2 \qquad (114)$$

over $x$

the value $x_0$ of $x$ that minimizes the Euclidean norm of the approximation error $e$ is

$$x_0 = (B^T B)^{-1} B^T c \qquad (115)$$

the matrix coefficient **c** being known as a *generalized inverse* of **B**, also known as the *left Moore-Penrose generalized inverse of* **B**. Therefore, several tests can be considered with this approach in order to evaluate the joint stiffness values. Moreover, if all joints are stressed substantially at least once among all the tests, their stiffness value will be accurately evaluated.

## 3.3 Developed method

In this section a method to get an *estimated* of values of stiffness is seen. The word *estimate* is used because with this method many of definitions are not applied, in contrast to state-of-art method. The choice of configuration must be done within the dexterity zone.

The application procedure for this method starts from the equation (57), reported above:

$$\begin{bmatrix} \dot{p}_e \\ \dot{\omega}_e \end{bmatrix} = J\,\dot{q} \qquad (116)$$

Performing a fundamental hypothesis, it is important to define finite increments and it is possible to write the following equation:

$$\begin{Bmatrix} \delta x \\ \delta y \\ \delta z \\ \delta \alpha \\ \delta \beta \\ \delta \gamma \end{Bmatrix}_j = J_j \begin{Bmatrix} \delta \theta_1 \\ \vdots \\ \delta \theta_6 \end{Bmatrix}_j \qquad (117)$$

the subscripts indicates j-th configuration.

Knowing the vector:

$$[\delta x \quad \delta y \quad \delta z \quad \delta \alpha \quad \delta \beta \quad \delta \gamma]^T \qquad (118)$$

From the linear system (117) the angles of joints are obtained, imposing a movement to end-effector. After obtaining the angles, we can obtain the torques of motors although the section 2.2.3.2, using the equation (64), it reported above:

$$\tau = J^T(q)\gamma_e \qquad (119)$$

After having obtained both the angles and the torques, it is sufficient to divide the torques and the angles, using the definition reported in the Equation 65:

$$K_i = \frac{\tau_i}{\delta \theta_1} \qquad (120)$$

As can be seen in the previous explanation, only three definitions were used for obtaining the stiffness values

# 4 Laboratory equipment : Manipulator, potentiometer and a mass

The laboratory equipment that is used will be discussed in this section. Laboratory equipment consist of the UR5 manipulator, the potentiometer and the payload.

## 4.1 The UR5 Manipulator

The UR5 is a manipulator manufactured by Universal Robots, with six degrees of freedom. It is part of lightweight robot category, and its weight is 18.4 kg. In the following table, the principal technical details are shown:

| Techinical details UR5 | |
|---|---|
| **Repeatability** | ±0,1 mm |
| **Payload** | 5 kg |
| **Reach** | 850 mm |
| **Degrees of freedom** | 6 rotating joints |
| **Working range of all joints** | ±360° |
| **Maximum speed of all joints** | ±180°/sec |
| **Footprint** | ø149mm |
| **Materials** | Aluminium, PP plastics |

*Table 1 - Techinical details of UR5 [11].*

*Figure 19 - UR5 Manipulators [11].*

The next section gives an overview of components, engaged in the UR5, and the employed control methods.

### 4.1.1 Components

In this section are analyzed only the joints components. Given that the links are composed of an appropriate section, it ensures a good compromise between the weight and the stiffness, and in this work the influence of links to the overall stiffness of UR5 has been neglected .

The principal components that compose the joints are:

- Brushless Servo Motor;
- Harmonic drive;

- Encoder;

### 4.1.1.1 Brushless Servo Motor

In the joints of UR5 a Brushless motor AC is incorporated. It is preferred to use compered to Brushless motor DC, because the characteristic of torque is constant. In fact, given that in the AC, winding power is supplied with a sinusoidal current so that the rotating field from the three three-phase currents is always offset by 90 ° electric from the rotor magnets field and by doing so the torque depends only of the power source.
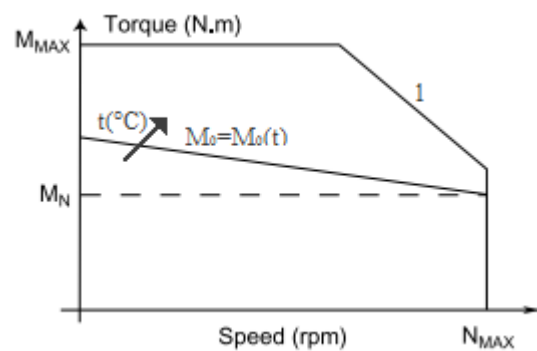


*Figure 20- Characteristic curve Brushless.*

where:

- $M_{MAX}$, maximum torque to avoid the motor demagnetization;
- $M_0$, stagnation torque, it is a temperature function;
- $M_N$, nominal torque;
- Tract 1,: saturation limit.

The main benefits of the use of motor Brushless are:

- The first significant benefit is the expected life of the engine, since the brushes are the "weak point" of an electric motor;
- The absence of brushes eliminates the main source of electromagnetic noise present in other electric motors;
- The loading gauge is limited in relation to the power that they can deliver and above all the torque that these engines can deliver;

- Permanent magnets are positioned on the rotor and are made with special materials that allow to have a very low rotor inertia, which allows to have extremely precise control both in speed and acceleration;
- Brushless engines always work in optimal performance, due to the fact that they don't have to generate the rotor magnetic field.



*Figure 21 – Motors Brushless[22]*

### 4.1.1.2    Harmonic Drive

The harmonic drives are particular reducers, which are chosen when compactness and low clearance are required. They are composed of three parts:

- **Circular spline:**  a steel cylinder with an internally teeth internally;
- **Flex spline:** a steel flexible cylinder with a teeth and a flanges for fitting;
- **Wave generator:** a thin ball bearing, mounted on an elliptical hub, in so doing we obtain a torque converter with good performance.
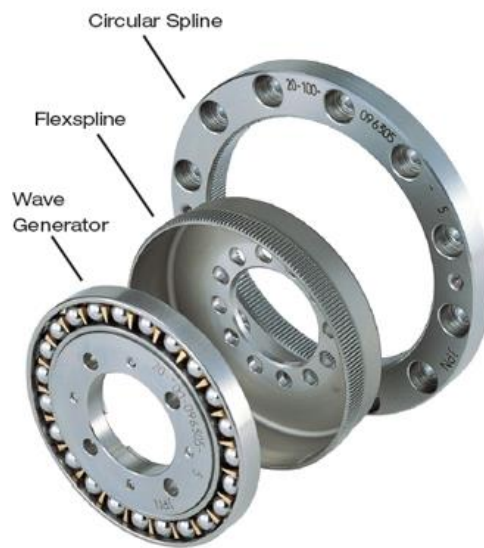
*Figure 22- Harmonic Drive[23].*

The flex spline has two teeth less than the circular spline. The flex spline should be kept in deformation from the wave generator. By rotating the wave generator , the engagement zone moves along with the major axis of the ellipse. When the wave generator has performed 180 degrees, the flex spline lag behind from circular spline of a tooth. Each complete revolution of wave generator moves the flex spline, that it is delaying behind of two-teeth compared to circular spline.

The principal benefits of the use of Harmonic drive are:

- Excellent positioning accuracy and repeatability;
- High capacity of torque transmission;
- Low clearance;
- High gear ratio with a single step: latter may vary from 50:1 to 320:1;
- Low wear;
- High torsional stiffness: the Harmonic Drive gearboxes show a high torsional rigidity throughout the range of speeds. The curve stiffness characteristic, virtually linear, guarantees excellent behavior during operation;

If $d$ is a total number of teeth of flex spline, the gear ratio is equal to:

$$n = -\frac{360°}{\frac{2}{d}360°} = -\frac{d}{2} \qquad (121)$$

Now, an introduction of an elasticity study is given to see the stiffness importance into the coupling motor-gearbox-power consumer. The equations describing the case study are three, one for each components:
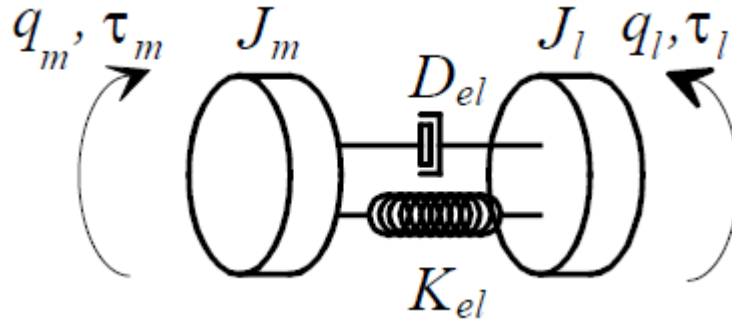


*Figure 103 - Dynamic model of motor- gearbox-power consumer*

motor $\qquad\qquad J_m\ddot{q}_m = \tau_m - \tau_{lm} \qquad\qquad (122)$

power consumer $\qquad\qquad J_l\ddot{q}_l = n\tau_{ml} - \tau_l \qquad\qquad (123)$

gearbox $\qquad\qquad \tau_{lm} = K_{el}(q_m - nq_l) + D_{el}(\dot{q}_m - n\dot{q}_l) \qquad (124)$

where:

$K_{el}$: torsional coefficient (Nm/rad);

$D_{el}$:dumping coefficient (Nms/rad);

$\tau_m$: motor torque;

$\tau_l$:power consumer torque;

$\tau_{lm}$: gearbox torque

### 4.1.1.3 Encoder

The operating principle of an absolute encoder is very similar to the incremental encoder, in which a rotating disc, with transparent and opaque areas, interrupts a beam of light acquired by photoreceptor.
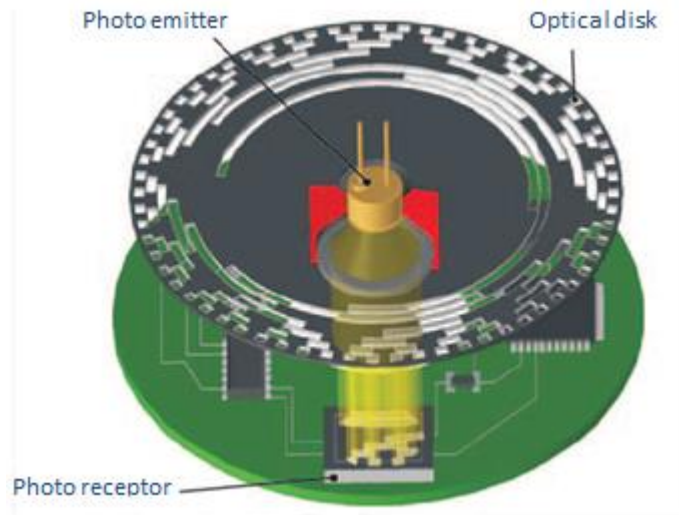


*Figure 114 – Encoder [Eltra]*

Compared to incremental encoders, absolute encoders have important functional differences. In fact in incremental encoders, the position is determined by the count of the number of pulses relative to the zero track, while in the absolute encoders position is determined by reading of the exit code. This last one is unique to each of the positions inside a lap. As a result, absolute encoders do not lose the real position when the power is removed, even in the case of movement, because of the use the Gray code and not the binary code as in incremental encoders.

### 4.1.1.4 Control Methods

The UR5 includes a controller platform with a teaching pendant that allows the user to program the robot using a graphical user interface. These programming interface constraints the options of control to Point-To-Point (PTP) movement in either joint-space or task-space. The default PTP movement is that the robot accelerates to the limited velocity, stays there for the maximum time allowed and decelerates to a halt when it reaches the implemented point in space. This results in a trapezoidal velocity trajectory.

Alternatively, the user can specify a blend radius, which gives the robot the freedom to deviate from the original path within circle around the programmed point. This allows the robot to keep a constant speed and drive through the desired path faster without stopping[13].
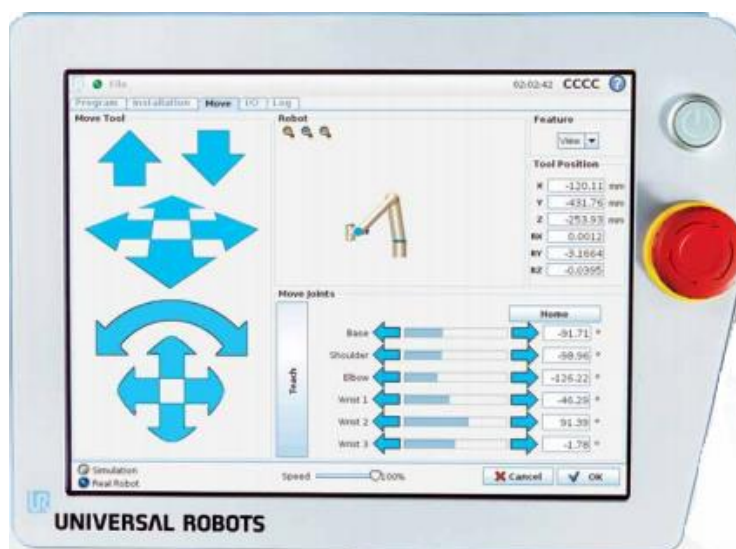


*Figure 125 - Controller UR5 [11]*

An alternative way to control the robot is to write programs in a scripting language called URScript, developed by the manufacturer. The programs can be saved directly on the robot controller or commands can be sent via a Transmission Control Protocol (TCP) socket to the robot. These programs are processed in the native high-level controller. It gives the user more options to customize a PTP movement in either joint-space or task-space [24].

A third way to control the robot is using the C programmed Application Programming Interface (C-API). This enables user coded C-programs to be executed and interact with the controller with a cycle time of 8 ms giving access to the low-level functions of the robot. More precisely, the Universal Robots servo controller can be controlled by either communicating joint velocities or a combination of joint positions, joint velocities and joint accelerations. As compared to the ways presented above to control the UR5, this method is not constrained by a superimposed velocity or acceleration profile and responds to commands quickly with a response delay time of only 12 ms. The preferred control method for research purposes is through the C-API as it gives most access to the control layers. However, the C-API has to be provided by the manufacturer. This was not the case

during the period of this study and it is unknown if access will be granted in the future. Therefore, the range of possibilities is currently constrained to the teaching pendant and the use of the scripting language URScript. As URScript allows a communication with the robot through an external personal computer (PC).

### 4.1.2 LX-PA wire potentiometer

The potentiometer is a transducer of movement based on the variation of resistance due to the movement of a mobile cursor. The potentiometer can be used as a voltage divider to obtain a manually adjustable output voltage at the slider (wiper) from a fixed input voltage applied across the two ends of the potentiometer. The characteristic equations are described below:

Eq. of partition

$$\frac{R_x}{R_L} = \frac{x}{L} \tag{125}$$

Eq. of functioning

$$V_O = R_x i = \frac{R_x}{R_L} V_s = \left(\frac{1}{L}\right) V_s \cdot x \tag{126}$$

Eq. of measure

$$x = \left(\frac{L}{V_s}\right) V_0 \tag{127}$$

Transfer function

$$\frac{V_O}{x} = \frac{V_s}{L} \tag{128}$$

$$i = V_S / R_L$$

$$i_0 = 0$$
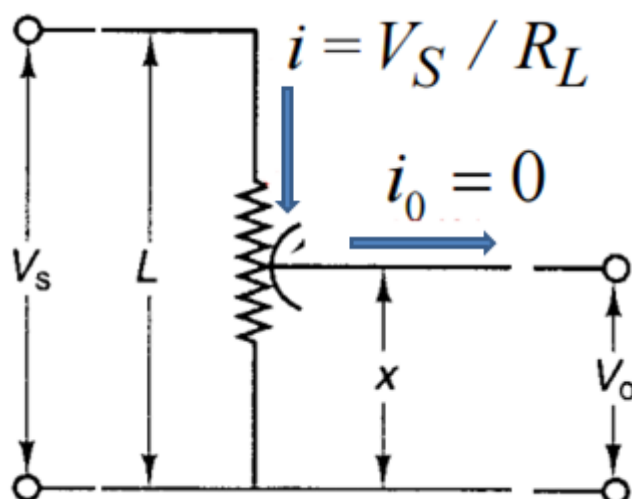
*Figure 26 – Diagram of operation potentiometer*

The operating principle has been explained with reference to linear potentiometer, but LX-PA used in this work is an angular potentiometer, where the wire connects the sensor and the measuring object in the direction of movement and it decouples the movement in the direction perpendicular to the wire (but is requires a correct alignment).



*Figure 27 -LX-PA wire potentiometer [SRP Control Systems]*

# 5 Evaluation of stiffness

## 5.1 UR5 parameters

The various models that are used to estimate the stiffness of the robotic joints are based on the kinematics shown in section 2.2. In this section the kinematic parameters of the UR5 that they are used to determine the stiffness of the joints are obtained.

### 5.1.1 Forward Kinematics

Figure 24 show an image of the UR5 manipulator with its joints and links. The manipulator has seven links $l_i: i \in \{0, \dots, 6\}$ and six revolute joints, $j_i: i \in \{1, \dots, 6\}$. Each revolute joint has one DOF, so the UR5 has a total of six DOF. The first step in order to derive the forward kinematics is to find the DH parameters.

### 5.1.2 DH Parameters

The DH parameters for the UR5 are derived according to the DH convention as presented in Section 2.2.2. The first step is to make a sketch of the manipulator with its joints and links, (see Figure 28);
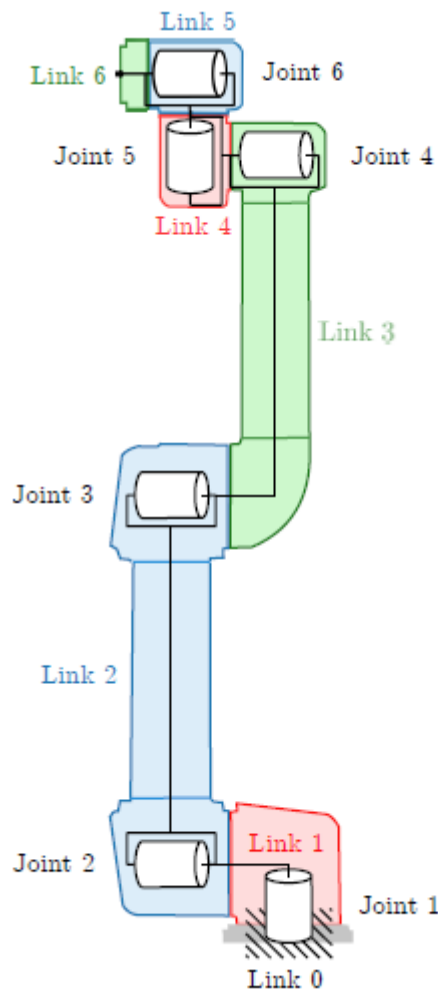
*Figure 28 - Sketch of the outer shape of the UR5 including its joints [25].*

The measurements of the size of the links are given by the manufacturer and were verified directly on the manipulator. Next, the coordinate frames $o_i x_i y_i z_i, \forall i \in \{0, \dots ,6\}$, are assigned based on the image and by complying with the DH convention. Figure 29 shows the assigned coordinate frames. Note that coordinate frame $o_2 x_2 y_2 z_2$ is not lying on the second link as this minimizes the number of non-zero DH parameters and makes the subsequent transformation matrices neat.
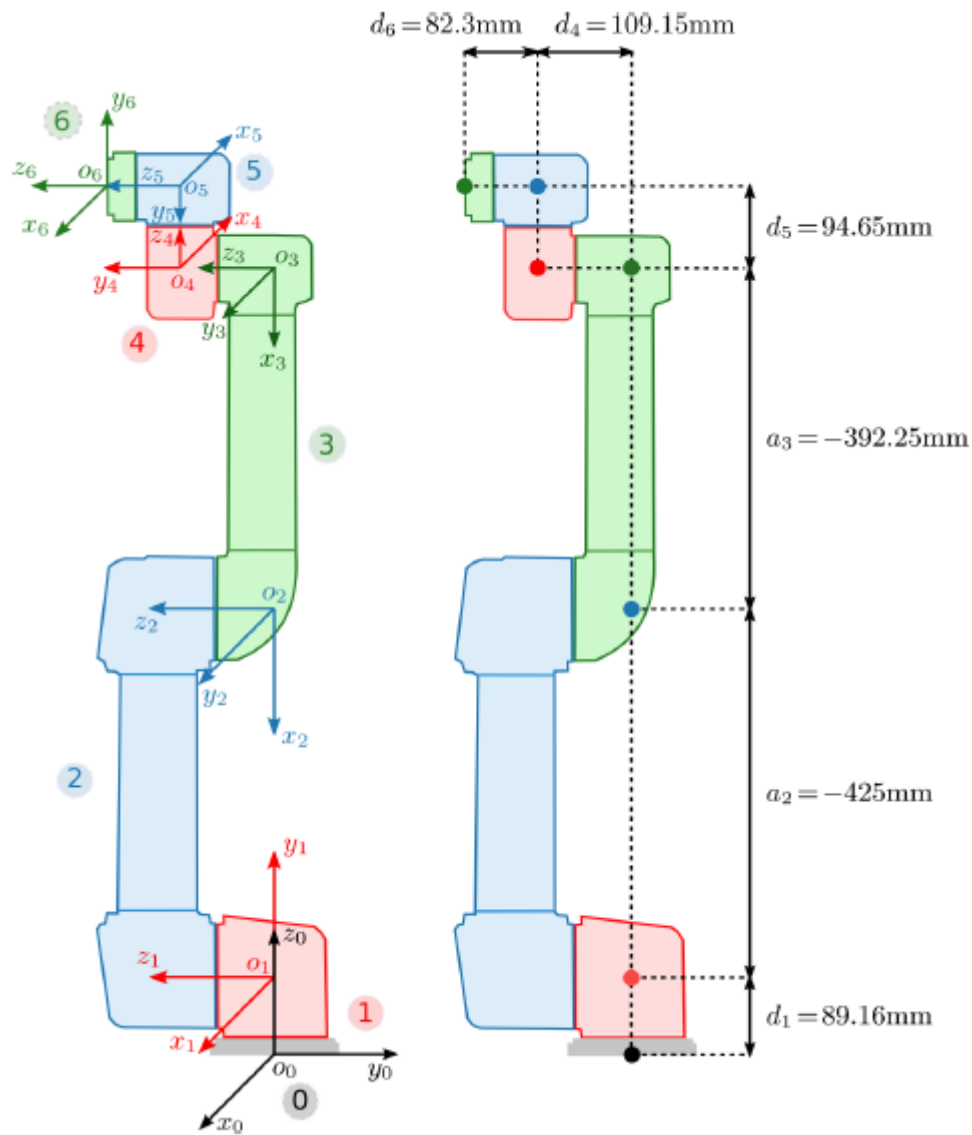
*Figure 29 - Sketch of the coordinate frames and Illustration*

*of the resulting DH parameters [25].*

Eventually the DH parameters are extracted using the assigned coordinate frames and the rules of the DH convention. They are shown in Figure 29 and summarized in table 2 and table 3.

| Link i | $\theta_i$ | $d_i$ | $a_i$ | $\alpha_i$ |
|--------|-----------|-------|-------|-----------|
| 1 | $\theta_1^*$ | $d_1$ | 0 | $\alpha_1$ |
| 2 | $\theta_2^*$ | 0 | $a_2$ | 0 |
| 3 | $\theta_3^*$ | 0 | $a_3$ | 0 |
| 4 | $\theta_4^*$ | $d_4$ | 0 | $\alpha_4$ |
| 5 | $\theta_5^*$ | $d_5$ | 0 | $\alpha_5$ |
| 6 | $\theta_6^*$ | $d_6$ | 0 | 0 |

Table 2 – Denavit- Hartenberg  parameters.

| Link i | $d_i \, [mm]$ | $a_i \, [mm]$ | $\alpha_i \, [rad]$ |
|--------|---------------|---------------|---------------------|
| 1 | 89.16 | 0 | $\pi/2$ |
| 2 | 0 | -425 | 0 |
| 3 | 0 | -392.25 | 0 |
| 4 | 109.15 | 0 | $\pi/2$ |
| 5 | 94.65 | 0 | $-\pi/2$ |
| 6 | 82.3 | 0 | 0 |

Table 3 - Denavit - Hartenberg values

### 5.1.3   Transformation Matrices

By inserting the parameters from Table 3 into Equation (10) the transformation matrices $T_1, \dots, T_6$ are obtained. They are

$$T_1 = \begin{bmatrix} R_1^0 & o_1^0 \\ \mathbf{0} & 1 \end{bmatrix} = \begin{bmatrix} \cos\theta_1 & 0 & \sin\theta_1 & 0 \\ \sin\theta_1 & 0 & -\cos\theta_1 & 0 \\ 0 & 1 & 0 & 89.16 \\ 0 & 0 & 0 & 1 \end{bmatrix} \qquad (129.a)$$

$$T_2 = \begin{bmatrix} R_2^1 & o_2^1 \\ \mathbf{0} & 1 \end{bmatrix} = \begin{bmatrix} \cos\theta_2 & -\sin\theta_2 & 0 & -425\cos\theta_2 \\ \sin\theta_2 & \cos\theta_2 & 0 & -425\sin\theta_2 \\ 0 & 0 & 1 & 0 \\ 0 & 0 & 0 & 1 \end{bmatrix} \qquad (129.b)$$

$$T_3 = \begin{bmatrix} R_3^2 & o_3^2 \\ 0 & 1 \end{bmatrix} = \begin{bmatrix} \cos\theta_3 & -\sin\theta_3 & 0 & -392\cos\theta_2 \\ \sin\theta_3 & \cos\theta_3 & 0 & -392\sin\theta_2 \\ 0 & 0 & 1 & 0 \\ 0 & 0 & 0 & 1 \end{bmatrix} \qquad (129.c)$$

$$T_4 = \begin{bmatrix} R_4^3 & o_4^3 \\ 0 & 1 \end{bmatrix} = \begin{bmatrix} \cos\theta_4 & 0 & \sin\theta_4 & 0 \\ \sin\theta_4 & 0 & -\cos\theta_4 & 0 \\ 0 & 1 & 0 & 109.15 \\ 0 & 0 & 0 & 1 \end{bmatrix} \qquad (129.d)$$

$$T_5 = \begin{bmatrix} R_5^4 & o_5^4 \\ 0 & 1 \end{bmatrix} = \begin{bmatrix} \cos\theta_5 & 0 & -\sin\theta_5 & 0 \\ \sin\theta_5 & 0 & \cos\theta_5 & 0 \\ 0 & -1 & 0 & 94.65 \\ 0 & 0 & 0 & 1 \end{bmatrix} \qquad (129.e)$$

$$T_6 = \begin{bmatrix} R_6^5 & o_6^5 \\ 0 & 1 \end{bmatrix} = \begin{bmatrix} \cos\theta_6 & -\sin\theta_6 & 0 & 0 \\ \sin\theta_6 & \cos\theta_6 & 0 & 0 \\ 0 & 0 & 1 & 82.3 \\ 0 & 0 & 0 & 1 \end{bmatrix} \qquad (129.f)$$

The forward kinematics are then described by the transformation matrix $T_6^0$ that describes the end effector position and orientation in terms of the base frame $o_0 x_0 y_0 z_0$ and the joint positions $\theta_1, \dots, \theta_6$. It is obtained by substituting Equations (129) into Equation (7) and results in

$$T_6^0 = T_1 T_2 T_3 T_4 T_5 T_6 = \begin{bmatrix} R_6^0 & o_6^0 \\ 0 & 1 \end{bmatrix} \qquad (130)$$

The resulting transformation matrix $T_6^0$ as well as the matrices in the following sections are omitted due to their size. In the following section the velocity kinematics are derived including the Jacobians geometric.

.

### 5.1.4 Velocity Kinematics-Geometric Jacobian

To calculate the angular part of the geometric Jacobian $\boldsymbol{J}_g$, namely $\boldsymbol{J}_{g,\omega}$, the axes from $z_0^0$ to $z_5^0$ are needed. They are obtained according to Equation (51) and result in

$$z_0^0 = \boldsymbol{z}_0 \tag{131.a}$$

$$z_1^0 = \boldsymbol{R}_1^0 \, \boldsymbol{z}_0 \tag{131.b}$$

$$z_2^0 = \boldsymbol{R}_2^0 \, \boldsymbol{z}_0 = \boldsymbol{R}_1^0 \, \boldsymbol{R}_2^1 \, \boldsymbol{z}_0 \tag{131.c}$$

$$z_3^0 = \boldsymbol{R}_3^0 \, \boldsymbol{z}_0 = \boldsymbol{R}_1^0 \, \boldsymbol{R}_2^1 \, \boldsymbol{R}_3^2 \, \boldsymbol{z}_0 \tag{131.d}$$

$$z_4^0 = \boldsymbol{R}_4^0 \, \boldsymbol{z}_0 = \boldsymbol{R}_1^0 \, \boldsymbol{R}_2^1 \, \boldsymbol{R}_3^2 \, \boldsymbol{R}_4^3 \, \boldsymbol{z}_0 \tag{131.e}$$

$$z_5^0 = \boldsymbol{R}_5^0 \boldsymbol{z}_0 = \boldsymbol{R}_1^0 \, \boldsymbol{R}_2^1 \, \boldsymbol{R}_3^2 \, \boldsymbol{R}_4^3 \, \boldsymbol{R}_5^4 \boldsymbol{z}_0 \tag{131.f}$$

Where $\boldsymbol{z}_0 = \begin{bmatrix} 0 & 0 & 1 \end{bmatrix}^T$ and where all $\boldsymbol{R}_{i+1}^i$ for $i \in \{0, \dots, 4\}$, are given in Equations (129). The linear part of the Jacobian, namely $\boldsymbol{J}_{g,v}$, is obtained as described in Equation (45). The geometric Jacobian is then

$$\boldsymbol{J}_g = \begin{bmatrix} \boldsymbol{J}_{g,v} \\ \boldsymbol{J}_{g,\omega} \end{bmatrix} = \begin{bmatrix} \boldsymbol{z}_0 \times (\boldsymbol{p}_e - \boldsymbol{p}_0) & \dots & \boldsymbol{z}_5 \times (\boldsymbol{p}_e - \boldsymbol{p}_5) \\ z_0^0 & \dots & z_5^0 \end{bmatrix} \tag{132}$$

Where $\boldsymbol{p}_e \in \mathbb{R}^3$ is the vector in the $4^{th}$ column of $\boldsymbol{T}_6^0$ in Equation (130).

## 5.2 Application of method adopted

### 5.2.1   Study of Dexterity

The study of dexterity is fundamental for the estimation of stiffness to learn about the zones where the hypothesis that, $K_c$ is negligible, is valid. The robot configurations for which the influence of $K_C$ on $K_X$ is higher when $k_F(J_N)^{-1}$ is minimum, close to singularity.

As seen above, section 3.2.1, the study of dexterity is done using the condition number of the Jacobian matrix, based on the Frobenius norm:

$$k_F(J_N) = \frac{1}{m}\sqrt{tr(J_N{}^T J_N)tr\left[(J_N{}^T J_N)^{-1}\right]} \tag{133}$$

where $J_N$ is the normalized Jacobian matrix of UR5, because the condition number of matrix **J** is meaningless, due to the fact that its terms are not homogeneous, not having the same unit.

The Jacobian is normalized by means of a normalizing length, latter is calculated as:

$$L \equiv \frac{R}{\bar{R}} \tag{134}$$

where $\bar{R} = \max_\theta\{\|\boldsymbol{p}_e - \boldsymbol{p}_0\|\}$, the maximum reach $\bar{R}$ of the UR5 manipulator, which is done by maximizing the distance of the operation point, namely end effector, of position vector $(\boldsymbol{p}_e - \boldsymbol{p}_0)$ from the first revolute axis. Apparently, the first and the last joint variable has no influence on this reach, and hence, can be locked at an arbitrary value, say of 0.

The value of $\bar{R}$ was implemented in MATLAB. The values of joints angles are:

| $\theta_1\,[deg]$ | $\theta_2\,[deg]$ | $\theta_3\,[deg]$ | $\theta_4\,[deg]$ | $\theta_5\,[deg]$ | $\theta_6\,[deg]$ |
|---|---|---|---|---|---|
| $0°$ | $-90°$ | $0°$ | $-90°$ | $0°$ | $0°$ |
| | $\bar{R}\,[mm]$ | | 1019.2 mm | | |

*Table 3*

and where R is the maximum reaches R of the actual manipulator, in the case of UR5, R=850mm[11]; thus L=0,8488 meter.

The study of dexterity is carried out for the second and the third revolute joints. They are the most influential joints on the translational motions of the end-effector and that the first revolute joint does not affect the robot dexterity. Therefore, let $\theta_1$ be null and the wrist angles $\theta_4, \theta_5$ and $\theta_6$ be set to 45° so that the corresponding wrist configuration is far from singularities.

| $\theta_1\,[deg]$ | $\theta_2\,[deg]$ | $\theta_3\,[deg]$ | $\theta_4\,[deg]$ | $\theta_5\,[deg]$ | $\theta_6\,[deg]$ |
|---|---|---|---|---|---|
| $0°$ | $0° \leq \theta_2 \leq 360°$ | $0° \leq \theta_3 \leq 360$ | $45°$ | $45°$ | $45°$ |

*Table 4*

Below the graphics of dexterity study of UR5 are given :
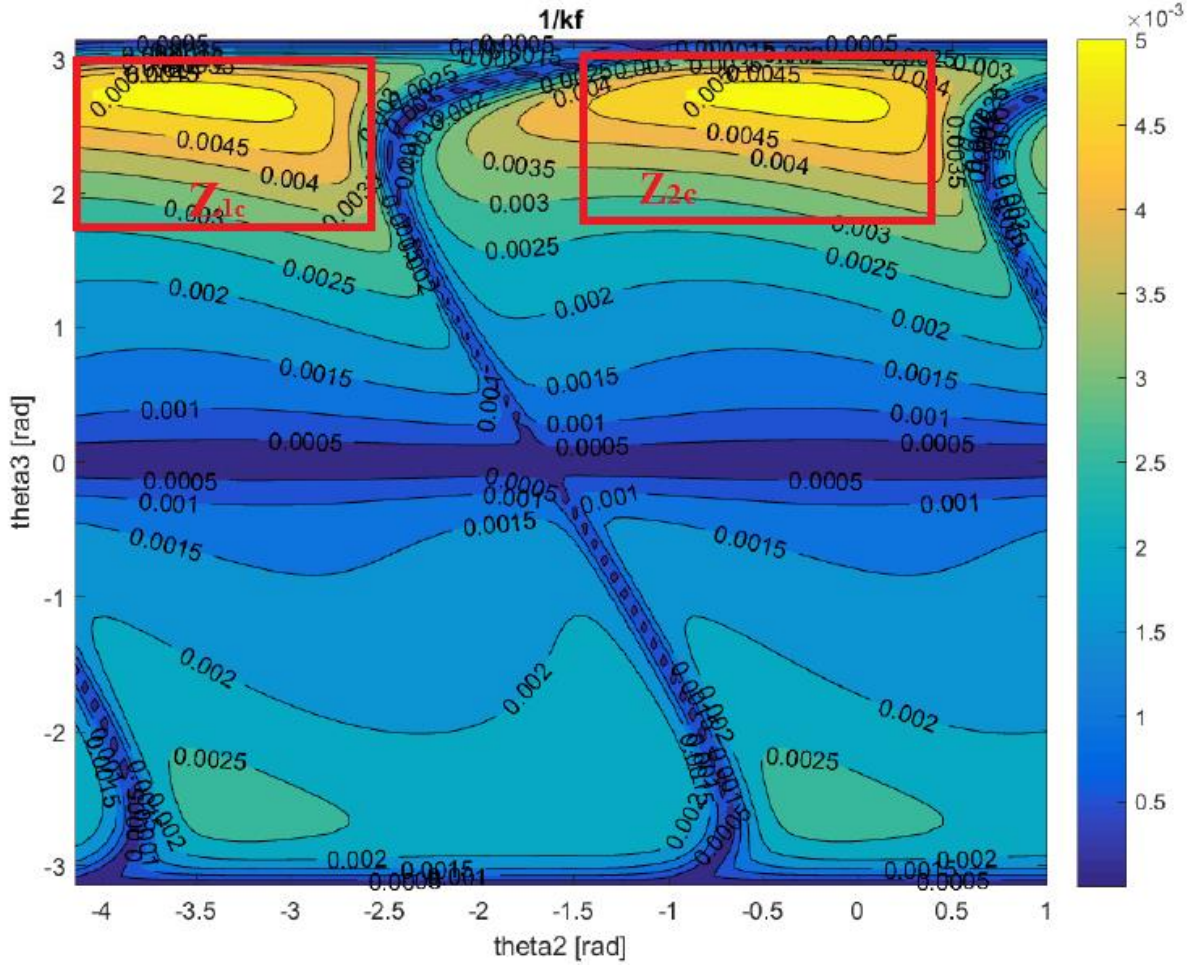
*Figure 30 - Contours of the inverse condition number of JN in the joint space*

The figure above shows the inverse condition number of $J_N$ with the assumptions of table 4. As we can see from figure, there are zones in the workspace where the $k_F(J_N)^{-1}$ assumes high values (0.0035-0.005), and where a good dexterity is associated. There are, also, zones in the workspace where the $k_F(J_N)^{-1}$ assumes low values (0.001-0.005) , in these areas there are the singularities.

The choice of configurations will be done in the areas with the best dexterity, in such a way that the Jacobian variation is negligible, in so doing, $K_C \approx 0$. The study of dexterity, recalled in the figure 28, shows four areas where the $k_F(J_N)^{-1}$ assumes acceptable values. For this work the chosen zones are $Z_{1c}$ and $Z_{2c}$, where the $k_F(J_N)^{-1}$ is higher.

The study of $k_F(J_N)^{-1}$ shows, however, a singularity for third angle joint equals zero, instead for second angle joint there are not defined values for the singularity, but it changes in the workspace.

| Zone | $\theta_2$ | $\theta_3$ |
|------|-----------|-----------|
| $Z_{1c}$ | -237° to -152° | 100° to 172° |
| $Z_{2c}$ | -89° to 23° | 100° to 172° |

*Table 5- The areas with the best dexterity.*

### 5.2.2 Evaluation of the joint stiffness values

Choosing the configurations within the dexterity zones, where the $k_F(J_N)^{-1}$ is maximum for the reason presented in the previous sections. The selected configuration are reported in the table below:

| N. test | $\theta_1$ [deg] | $\theta_2$ [deg] | $\theta_3$ [deg] | $\theta_4$ [deg] | $\theta_5$ [deg] | $\theta_6$ [deg] |
|---------|--------|--------|--------|--------|--------|--------|
| 1 | 0° | -237° | 119° | 45° | 0° | 71.9° |
| 2 | 17° | -162° | 137° | 39° | 25° | -14.4° |
| 3 | 15.5° | -177° | 149° | 45° | 25° | -17° |
| 4 | 0° | -183° | 139° | 45° | 25° | -51° |
| 5 | 13° | -199° | 143° | 37° | 0° | 17.1° |
| 6 | 7° | -223° | 123° | 45° | 6° | 54.6° |

*Table 6- The selected configurations*



*Figure 31- Configuration 1 [26]*

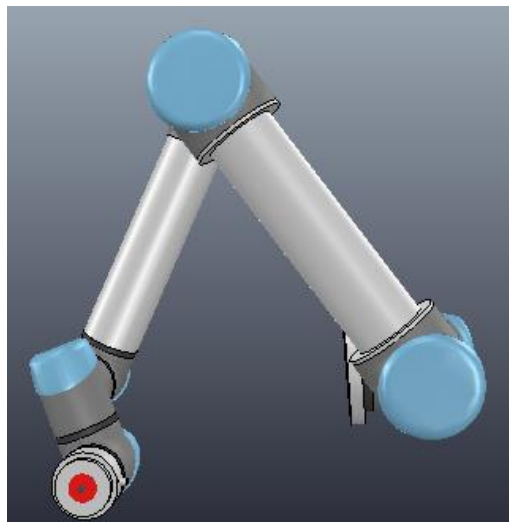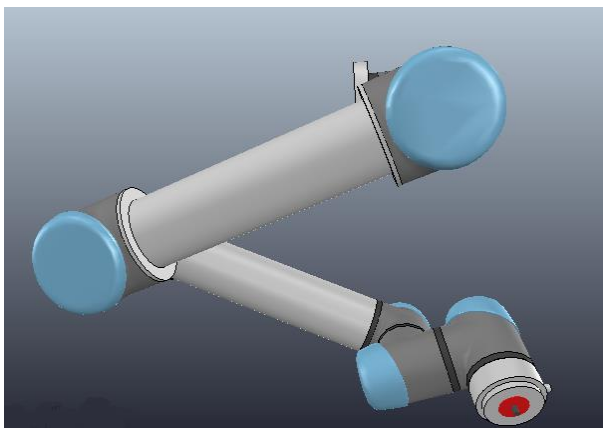*Figure 32- Configuration 2 [26]*
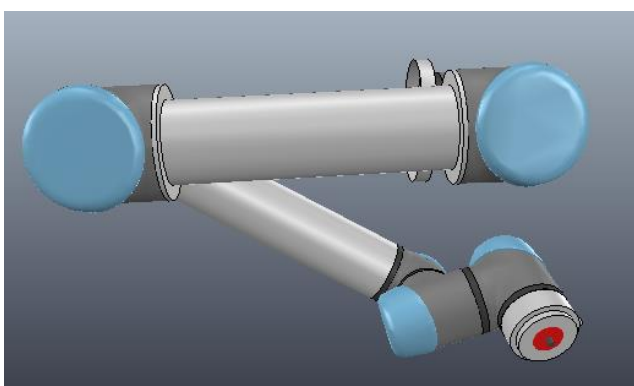


*Figure 33- Configuration 3 [26]*
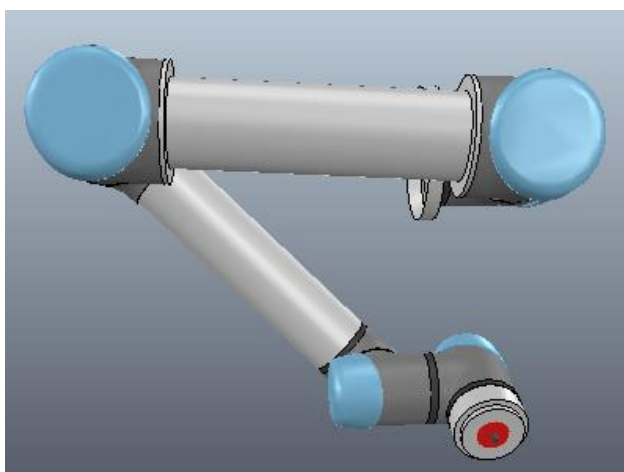


*Figure 34 - Configuration 4 [26]*
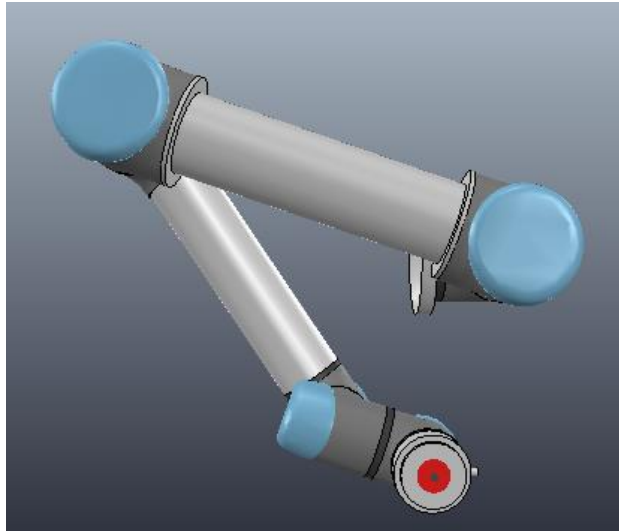
*Figura 35 - Configuration 5 [26]*
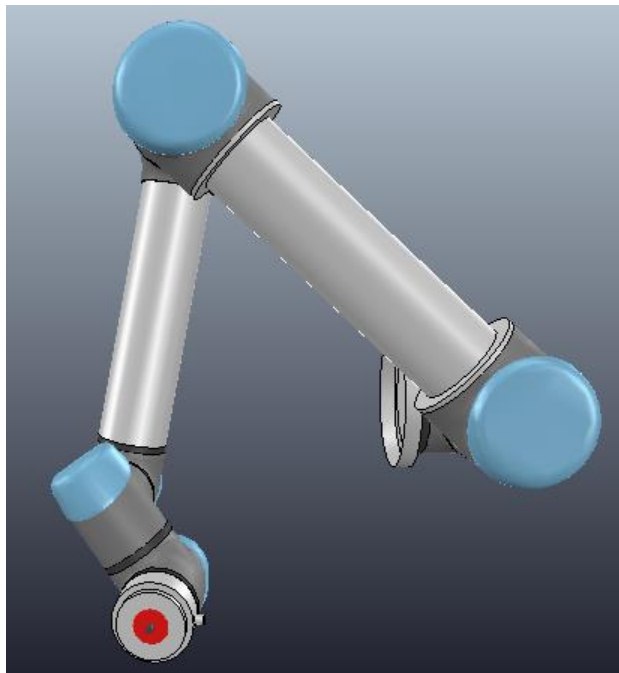


*Figura 36 - Configuration 6 [26]*

Now, the end effector is loaded with a payload , in this case $\boldsymbol{F} = m * g = 18.6718\ N$, in order to facilitate application of force, the cantilever was mounted in the end-effector.

*Figure 37 - Configuration with the system of loading.*

After placing the weight in the cantilever, through the LX-PA wire potentiometer, the displacement was measured . This measurement provides the $\delta d$.

The measurement was conducted in the following way:

1. The robot is positioned in the selected configuration;
2. The wire potentiometer can measure only in one direction. The selected direction has components along the X axis and along the Y axis of end effector frame;
3. The end-effector pose is measured without payload;
4. The payload is put in the cantilever, and the measures are repeated;
5. Every measurement is repeated six times for every configuration;
6. Changing the configuration of wire potentiometer is checked to see if the component along with Z axis is negligible compared with X and Y components.

The measurement are reported below:

| First configuration | | | | | | |
|---|---|---|---|---|---|---|
| N.test | 1 | 2 | 3 | 4 | 5 | 6 |
| Without payload [mm] | 0,001 | 0,010 | 0,005 | -0,002 | 0,001 | -0,010 |
| With payload [mm] | -0,202 | -0,206 | -0,220 | -0,228 | -0,225 | -0,225 |
| deflection | 0,203 | 0,216 | 0,225 | 0,226 | 0,226 | 0,215 |

*Table 7*

| Second configuration | | | | | | |
|---|---|---|---|---|---|---|
| N.test | 1 | 2 | 3 | 4 | 5 | 6 |
| Without payload [mm] | -0.068 | -0.068 | -0.079 | -0.066 | -0.074 | -0.075 |
| With payload [mm] | -0,122 | -0,122 | -0,121 | -0,125 | -0.124 | -0.123 |
| deflection | 0,054 | 0,054 | 0,042 | 0,059 | 0.05 | 0.048 |

*Table 8*

| Third configuration | | | | | | |
|---|---|---|---|---|---|---|
| N.test | 1 | 2 | 3 | 4 | 5 | 6 |
| Without payload [mm] | 0,287 | 0,276 | 0,287 | 0,266 | 0.28 | 0.272 |
| With payload [mm] | 0,208 | 0,207 | 0.205 | 0.207 | 0.209 | 0.205 |
| deflection | 0,079 | 0,069 | 0,082 | 0,059 | 0.071 | 0.067 |

*Table 9*

| Fourth configuration | | | | | | |
|---|---|---|---|---|---|---|
| N.test | 1 | 2 | 3 | 4 | 5 | 6 |
| Without payload [mm] | -0.011 | -0.032 | -0.025 | -0.020 | -0.029 | -0.024 |
| With payload [mm] | -0.128 | -0.132 | -0.139 | -0.153 | -0.152 | -0.125 |
| deflection | 0.117 | 0.100 | 0.114 | 0.133 | 0.123 | 0.134 |

*Table 10*

| Fifth configuration | | | | | | |
|---|---|---|---|---|---|---|
| N.test | 1 | 2 | 3 | 4 | 5 | 6 |
| Without payload [mm] | 0.094 | 0.093 | 0.085 | 0.084 | 0.090 | 0.087 |
| With payload [mm] | 0.069 | 0.070 | 0.065 | 0.068 | 0.071 | 0.072 |
| deflection | 0,025 | 0,023 | 0,020 | 0.016 | 0.019 | 0.015 |

*Table 11*

| Sixth configuration | | | | | | |
|---|---|---|---|---|---|---|
| N.test | 1 | 2 | 3 | 4 | 5 | 6 |
| Without payload [mm] | 0,072 | 0,057 | 0,042 | 0.056 | 0,054 | 0.047 |
| With payload [mm] | -0,133 | -0,147 | -0,136 | -0,136 | -0,144 | -0,143 |
| deflection | 0,205 | 0,204 | 0,178 | 0,192 | 0,198 | 0,190 |

*Table 12*

The displacement along Z axis is over the resolution of LX-PA for every configuration and the displacement in the above tables has component along X and Y, respectively to 45° and 45°.

Considering the force applied to end-effector and the frame of the latter, we can obtain the vector $\gamma_e$ of external forces and moments exerted on the robot end-effector. In this case is follows:

$$\gamma_e = [13.20N \quad 13.20N \quad 0 \quad 0 \quad 0 \quad 9.336\ Nm] \tag{135}$$

As seen in the section( 3.2.2) the matrix **A** is obtained knowing the Jacobian and the vector $\gamma_e$, using the equation (110). In the end we can use the equation (114) to determine the compliance, and consequently the stiffness:
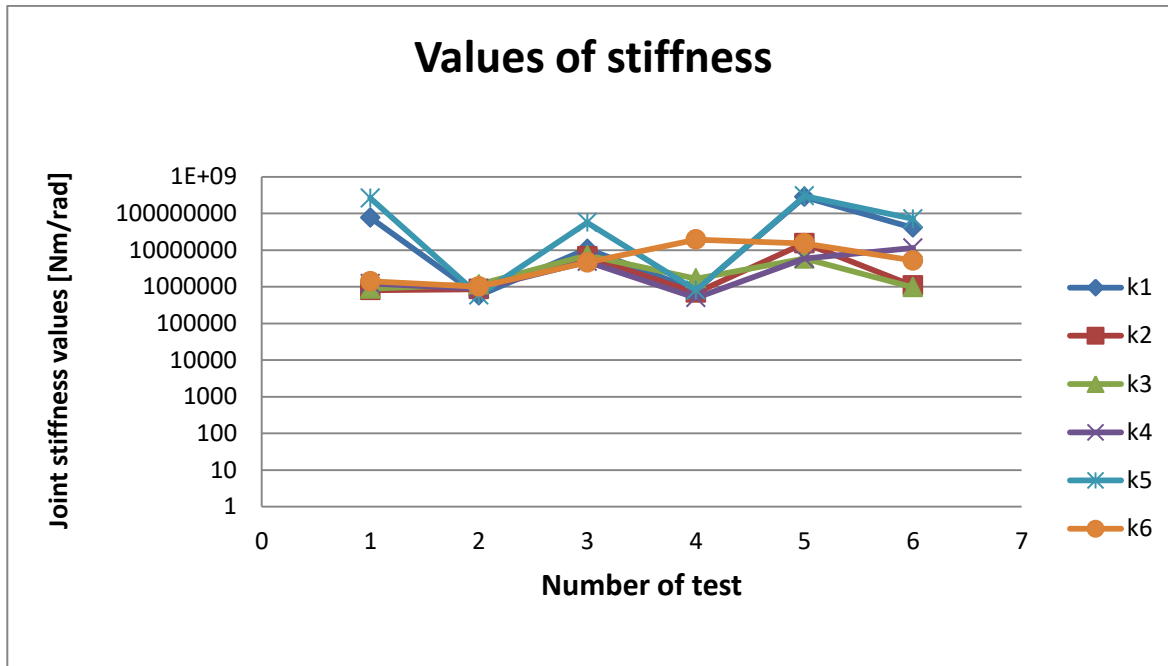
*Figure 38 – Results of adopted method*

The variance of the results is due to the incorrect choice of wrist position, to allow the measure of end-effector displacement and to allow the application of load in the end-effector. The wrist was placed, inevitably, in different positions in respect to the table 4..

To see the importance of dexterity study, which makes possible to choose the corrects configurations, where $K_c$ is negligible, below it is reported a calculation of stiffness choosing others configurations out of the zone the dexterity:

| N. test | $\theta_1 \, [deg]$ | $\theta_2 \, [deg]$ | $\theta_3 \, [deg]$ | $\theta_4 \, [deg]$ | $\theta_5 \, [deg]$ | $\theta_6 \, [deg]$ |
|---------|------|------|------|------|------|------|
| 1 | 65° | -18° | 90° | -65° | -110° | 1.2° |
| 2 | 94° | -20° | -97° | -157° | -46.98° | -224 ° |
| 3 | 135° | 35° | -112° | -49° | -239° | -15° |
| 4 | 182° | 18° | -122° | -122° | 90.5° | -45° |
| 5 | 221° | -18° | -56° | -58° | -27.8° | -41° |

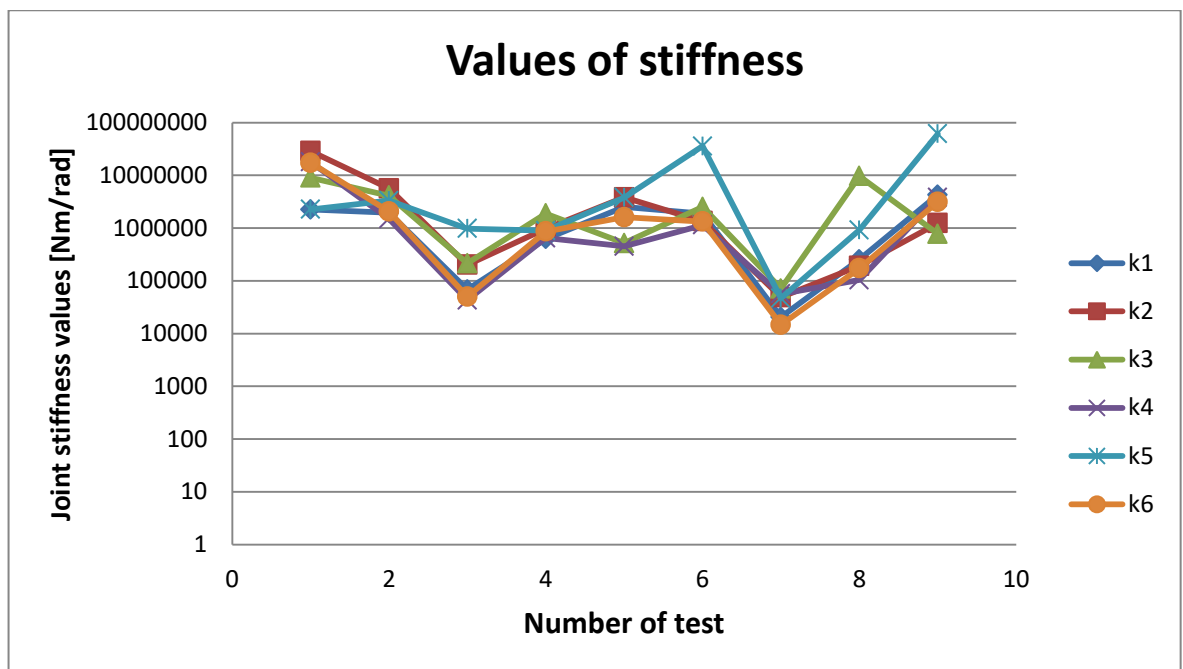| 6 | 273° | -16° | 115° | -186° | -135° | -15 |
| 7 | 67° | -173° | 128° | -19° | -40° | 131° |
| 8 | 109° | -131° | 62° | -37° | 41° | -95° |
| 9 | 86° | -10° | 56° | -132° | -47° | -43° |

*Table 13*



*Figure 39 - Results outside dexterity zones*

Moreover, to realize the validity of mathematical model and the weight of adopted hypothesis is given a figure (Figure 40), where the wrist joint angles have set on 45°, as in the dexterity analysis assumed and the end-effector displacements where chosen dimensionally consistent:
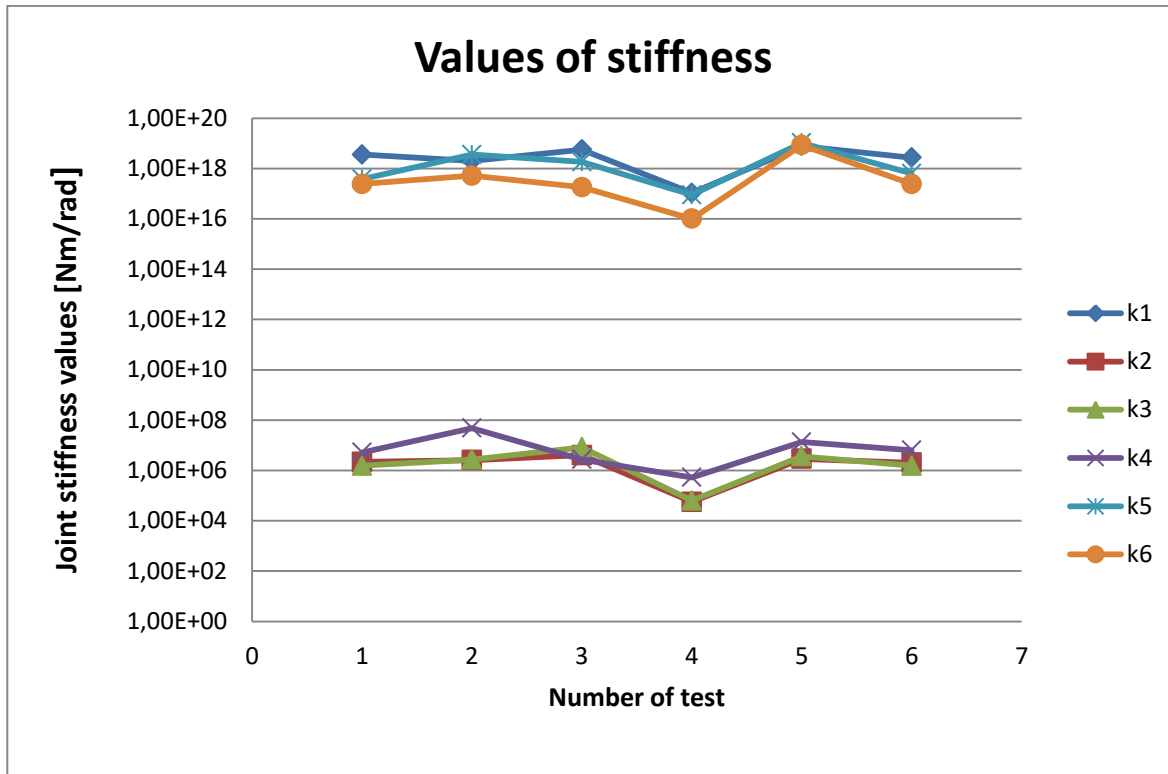
Figure 40 - Results without simplifying assumptions

It is apparent that the variations in the obtained joint stiffness values is reasonably small, the method for the joint stiffness identification is robust. Moreover, clearly more tests are conducted more the results are reliable.

## 5.3 Application of the developed method

Following the section 3.3 we can calculate the stiffness of the Joints, but the employed sensor (LX-PA wire potentiometer) allows us to measure only a displacement, therefore we introduce some hypothesis for allowing the stiffness calculate.

For the application of developed method are necessary the three displacements and three rotations, but with the sensor LX-PA, it is possible to know only the displacements. Through a further measurement it is possible to know the rotation along the Z axis. The further measurement has taken in the end of cantilever, in so doing is possible to obtain the rotation along Z axis knowing the length of cantilever and the end effector displacement .

Now, under the assumption that the rotations along Y and X are negligible respect to rotation along Z due to the robot configurations taken. Finally the joint angle values are obtained.

| First configuration | | | | | | |
|---|---|---|---|---|---|---|
| N.test | 1 | 2 | 3 | 4 | 5 | 6 |
| Without payload [mm] | 0,101 | 0,110 | 0,105 | 0,098 | 0,101 | 0,110 |
| With payload [mm] | -0,402 | -0,406 | -0,420 | -0,428 | -0,425 | -0,425 |
| deflection | 0,301 | 0,296 | 0,315 | 0,33 | 0,324 | 0,315 |

*Table 14*

| Second configuration | | | | | | |
|---|---|---|---|---|---|---|
| N.test | 1 | 2 | 3 | 4 | 5 | 6 |
| Without payload [mm] | -0.168 | -0.168 | -0.179 | -0.166 | -0.174 | -0.175 |
| With payload [mm] | -0,522 | -0,522 | -0,521 | -0,525 | -0.524 | -0.523 |
| deflection | 0,354 | 0,354 | 0,342 | 0,359 | 0.35 | 0.348 |

*Table 15*

| Third configuration | | | | | | |
|---|---|---|---|---|---|---|
| N.test | 1 | 2 | 3 | 4 | 5 | 6 |
| Without payload [mm] | 0,287 | 0,276 | 0,287 | 0,266 | 0.28 | 0.272 |
| With payload [mm] | 0,508 | 0,507 | 0.505 | 0.507 | 0.509 | 0.505 |
| deflection | 0,221 | 0,231 | 0,218 | 0,241 | 0.229 | 0.233 |

*Table 16*

| Fourth configuration | | | | | | |
|---|---|---|---|---|---|---|
| N.test | 1 | 2 | 3 | 4 | 5 | 6 |
| Without payload [mm] | -0.051 | -0.082 | -0.075 | -0.070 | -0.079 | -0.074 |
| With payload [mm] | -0.229 | -0.238 | -0.246 | -0.240 | -0.258 | -0.245 |
| deflection | 0.178 | 0.156 | 0.171 | 0.17 | 0.179 | 0.171 |

*Table 17*

| Fifth configuration | | | | | | |
|---|---|---|---|---|---|---|
| N.test | 1 | 2 | 3 | 4 | 5 | 6 |
| Without payload [mm] | 0.194 | 0.193 | 0.185 | 0.184 | 0.190 | 0.187 |
| With payload [mm] | 0.380 | 0.382 | 0.379 | 0.372 | 0.375 | 0.381 |
| deflection | 0,186 | 0,189 | 0,194 | 0.188 | 0.185 | 0.194 |

*Table 18*

| Sixth configuration | | | | | | |
|---|---|---|---|---|---|---|
| N.test | 1 | 2 | 3 | 4 | 5 | 6 |
| Without payload [mm] | 0,093 | 0,078 | 0,063 | 0.078 | 0,079 | 0.068 |
| With payload [mm] | -0,454 | -0,444 | -0,439 | -0,439 | -0,448 | -0,441 |
| deflection | 0,547 | 0,522 | 0,502 | 0,517 | 0,527 | 0,509 |

*Table 19*

Also in this case, the displacement along Z axis is over the resolution of LX-PA for every configuration and the displacement in the above tables has component along X and Y, respectively to 45° and 45°.

Now, applying the procedure exposed in the section 2.2.3.2 is possible to obtain the torque that each joints must oppose to maintain the static equilibrium, when in the end- effector is applied a force or a torque.

Through the Equation (64) is obtained the 6-dimensional vector $\tau$, having previously the Jacobian and by breaking down the components of vector force with regard to frame of end-effector.

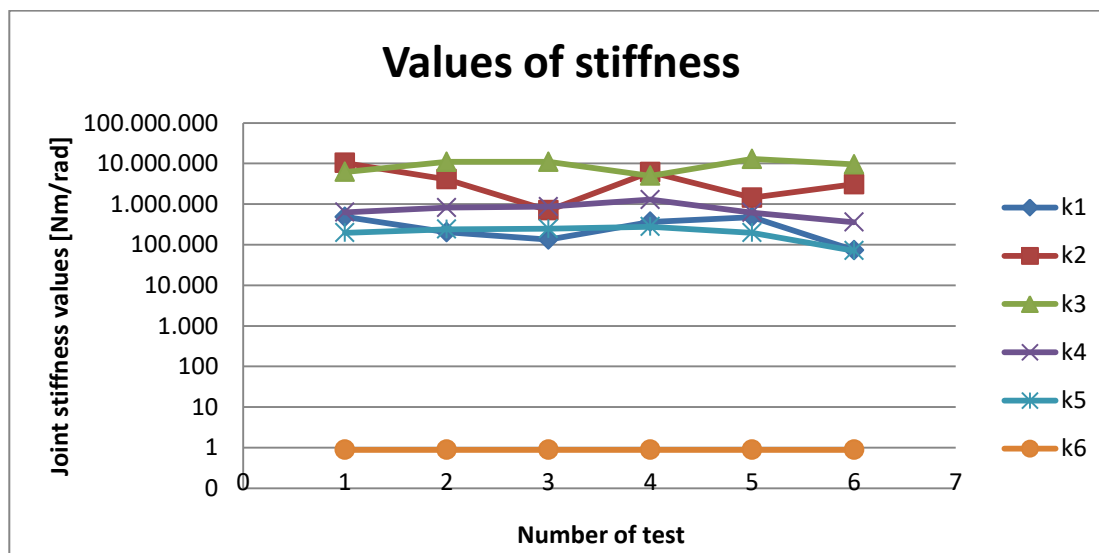Using the Equation 120, the stiffness of Joints are obtained and they are shown in the following graph:



*Figure 41 - Results of developed method*

## 5.4    Analysis of the results

In this section are analyzed the results that have been obtained with the state-of-art and the developed method. Beginning with the state-of-art method, we can see the importance of choice of configurations within of dexterity zone. In fact, by comparing the Figure 38, Figure 39 and Figure 40 the variation of results is smaller for every joints. In the latter case the configurations are not in zones of dexterity.

However, in the first case (Figure 38), the limit of measurement system did not allow to position the wrist far of singularity, therefore also the first case will have a variation of results. In fact the figure 40 shows that which would be produced if the configurations were corrects , a possible option of measurement system the laser tracker instead potentiometer.

In the developed method the results present a variation less than the state-of-art method. Nevertheless the measuring system (LX-PA) allows to measure the three translations $(\delta x, \delta y, \delta z)$ and it doesn't allow to know directly the three rotations $(\delta \alpha, \delta \beta, \delta \gamma)$. With the way exposed in the section 5.3 it is possible to know the rotation along Z axis.

In the figure 41 it is possible to see the results of developed method, the particular result of the last stiffness joint value is given by proximity of wrist to singularity configuration. Nevertheless the results variation is smaller than the state-of-method, Although these changes were goods, caution should be exercised when the Jacobian matrix is ill-conditioned, for this reason the configurations should be chosen far to singularity position of robot.

The comparison  of two method would not lead to any information until the sources of errors will not be deleted or minimized.

# 6 Conclusions

The goal of this project was to know the stiffness values of joint through both a developed method and state-of-art method. The results, which have been obtained with implemented method, were compared with an state-of-art method from bibliography.

Experimental measurements were conducted to estimate the stiffness on each joint, from which it is seen the importance of dexterity zone. The dexterity zone in the work space of URL5 is detected in a mathematical way, and based on this results, the configuration of measures should be selected.

Having chosen the configurations of the robot in the dexterity zone, a sufficient number of tests[8] were conducted to apply both the developed method and the state-of-art method,. By the variation of results was observed that the employed sensor (LX-PA wire potentiometer) does not allow the sufficient accuracy.

The methods show a discrepancy of values due to the sources errors. Both methods require a high number of tests in such a way that the stiffness values will result as accurate as can be.

However, one fundamental conclusion is that the measurement system is of fundamental importance for inspection work, like that conducted in this work

For future work a proof of results may be conducted by extrapolating a reading of angles from the encoder, that should be positioned on each joint.

---

[8] sufficient number of tests: six tests are chosen in the thesis work, if the tests conducted are sufficiently high, it is possible to calculate an average for every stiffness joint value

# Bibliography

**[1]** RIVIN E.I., "Stiffness and Damping in Mechanical Design", Marcel Dekker Inc., New York,1999.

**[2]** TSAI L.W., "Robot Analysis: The Mechanics of Serial and Parallel Manipulators", John Wiley & Sons, New York, 1999.

**[3]** CIBLAK N., LIPKIN H., "Synthesis of Cartesian Stiffness for Robotic Applications", Proceedings of the IEEE International Conference on Robotics and Automation ICRA'99, Detroit, vol.3, pp.2147-2152, 1999.

**[4]** Selig J.M., "The Spatial Stiffness Matrix from Simple Stretched Springs", Proceedings of the IEEE International Conference on Robotics and Automation ICRA'00, San Francisco, vol.4, 2000.

**[5]** PIGOSKI T., GRIFFIS M., DUFFY J., "Stiffness Mappings Employing Different Frames of Reference", Mechanism and Machine Theory, vol.33, n.6, pp.825-838, 1998.

**[6]** HUANG S., SCHIMMELS J.M., "The Eigenscrew Decomposition of Spatial Stiffness Matrices",IEEE Transactions on Robotics and Automation, vol.16, n.2, 2000.

**[7]** VAISHNAV R.N., MAGRAB E.B., "A General Procedure to Evaluate Robot Positioning Errors", International Journal of Robotics Research, vol.6, n.1, pp.59-74, 1987.

**[8]** KIM H.Y., STREIT D.A., "Configuration Dependent Stiffness of the Puma 560 Manipulator: Analytical and Experimental Results", Mechanism and Machine Theory, vol.30, n.8, 1995.

**[9]** BRUNO SICILIANO, LORENZO SCIAVICCO, LUIGI VILLANI, GIUSEPPE ORIOLO, Robotics, Modelling, Planning and Control, 2009, Springer-Verlag London Limited, Pages 58-65, Pages 105-113, Pages 147-148.

**[10]** SHIMON Y. NOF, Handbook of industrial robotics, Editor school of industrial engineering Purdue University West Lafayette, Indiana, 1985, John Wiley & Sons, Inc. Pages

32-37.

**[11]**    www.universal-robots.com

**[12]**    H. ASADA, J.-J. E. SLOTINE, Robotic Analysis and control, 1986, John Wiley & Sons, Inc. Pages 86-92.

**[13]**    SERVICE MANUAL, Revision UR5_en_3.1.3

**[14]**    ABELE, E., WEIGOLD, M. AND ROTHENBCHER, S. (2007). "Modeling and Identification of an Industrial Robot for Machining Applications," Elsevier,  Annals of the CIRP, 56/1/2007.

**[15]**    CHEN, S.-F. (2003). "The 6x6 Stiffness Formulation and Transformation of Serial Manipulators via the CCT Theory," IEEE International Conference on Robotics & Automation, Taiwan**.**

**[16]**    CLAIRE DUMAS, STÉPHANE CARO, CHERIF MEHDI, SÉBASTIEN GARNIER, BENOÎT FURET, Joint Stiffness identification of Industrial Serial Robots. Robotica, Cambridge University Press, 2011, pp.1-20.

**[17]**    OLIVER PORGES, ROBERTO LAMPARIELLO, JORDI ARTIGAS, ARMIN WEDLER, CHRISTOPH BORST, MAXIMO A. ROA" Reachability and Dexterity: Analysis and Applications for Space Robotics" German Aerospace Center (DLR), 82234 Wessling, Germany.

**[18]**    RAYMOND R. MA AND AARON M. DOLLAR "On Dexterity and Dexterous Manipulation"

**[19]**    DARIO A. BINI, "Norme di vettore e di matrici", Università di Pisa, 30 ottobre 2013, pp.7-10.

**[20]**    RANJBARAN, F., ANGELES, J., González-Palacios, M. A., and Patel, R. V., 1995, "The Mechanical Design of a Seven-Axes Manipulator With Kinematic Isotropy," J.Intell. Robotic Syst., 14, pp. 21–41.

**[21]**    KHAN, W.A. AND ANGELES, J. (2006). "The Kinetostatic Optimization of Robotic Manipulators: The Inverse and the Direct Problems," ASME Journal of Mechanical Design, 128, pp. 168–178.

**[22]**    http://www.lafert.com.

**[23]**    https://harmonicdrive.de/it

**[24]**    Universal Robots. The URScript Programming Language, February 2013

**[25]**    KATHARINA KUFIETA, Force Estimation in Robotic Manipulators: Modeling, Simulation and Experiments, NTNU, Department of Engineering Cybernetics NTNU Norwegian University of Science and Technology.

**[26]**    Produced with V-REP software